

AMERICAN UNIVERSITY OF BEIRUT

IMPACT OF EVAPOTRANSPIRATION AND BIOMASS  
MODEL SELECTION ON IRRIGATION ECONOMICS:  
WAPOR, HSEB, AND GYMEE. INSIGHTS FROM THE  
LITANI RIVER BASIN

by  
RIM ALI HAZIMEH

A thesis  
submitted in partial fulfillment of the requirements  
for the degree of Master of Science  
to the Department of Agriculture  
of the Faculty of Agricultural and Food Sciences  
at the American University of Beirut

Beirut, Lebanon  
October 2023

AMERICAN UNIVERSITY OF BEIRUT

IMPACT OF EVAPOTRANSPIRATION AND BIOMASS  
MODEL SELECTION ON IRRIGATION ECONOMICS:  
WAPOR, HSEB, AND GYMEE. INSIGHTS FROM THE  
LITANI RIVER BASIN

by  
RIM ALI HAZIMEH

Approved by:

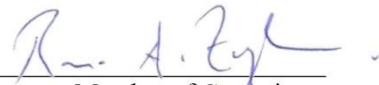
Dr. Hadi Jaafar, Associate Professor  
Department of Agriculture

Hadi Jaafar

Digitally signed by Hadi Jaafar  
DN: cn=Hadi Jaafar, o=American  
University of Beirut, ou=Department of  
Agriculture, email=hj21@aub.edu.lb,  
c=LB  
Date: 2023.10.09 09:34:24 +03'00'

Advisor

Dr. Rami Zurayk, Professor  
Department of Landscape Design  
and Ecosystem Management



Member of Committee

Dr. Ali Chalak, Associate Professor  
Department of Agriculture



Member of Committee

Date of thesis defense: October 5, 2023



## ACKNOWLEDGEMENTS

I thank God for granting me the strength and perseverance to reach this milestone. I am deeply grateful to all those who have played a pivotal role in the successful completion of this thesis.

A special acknowledgment goes to my dedicated supervisor, Dr. Hadi Jaafar, whose expert guidance, and commitment to my academic growth have been invaluable. I express my appreciation to my committee members, Dr. Rami Zurayk and Dr. Ali Chalak, for their constructive criticism, which has improved the quality of this thesis.

I extend my heartfelt thanks to my lab mates, Lara Sujud, Batoul Wehbe, Abdul Razzak Doughan, Georges Rahal, and my cousin Adam Hazimeh, whose presence and support made the long hours in the lab not only bearable, but also enjoyable. A special thanks goes to Lara, whose invaluable insights and thought-provoking discussions enriched the quality of my work.

I owe a debt of gratitude to my parents, Hala and Ali, whose boundless encouragement and sacrifices paved the way for my education. Your belief in my potential has always pushed me to strive for excellence.

To my wonderful sister Rana and brother Ahmad, your motivation has always been right by my side. I am lucky to have siblings who are a constant source of inspiration.

To my beloved fiancé Abed Yehya, your patience, love, and understanding sustained me during this challenging academic pursuit. I salute the countless cups of coffee we shared while discussing and brainstorming ideas. Your presence and support have made all the difference.

Lastly, I extend my profound thanks to my genuine friends Ghida, Aya, Lorena, and Sabrina who have always made the pursuit of knowledge meaningful and joyful.

# ABSTRACT OF THE THESIS OF

Rim Ali Hazimeh

for

Master of Science  
Major: Irrigation

Title: Impact of Evapotranspiration and Biomass Model Selection on Irrigation Economics: WaPOR, HSEB, and GYMEE. Insights from the Litani River Basin

Using Economic Irrigation Water Productivity (EIWP) as an indicator for on-farm irrigation decision-making is of utmost importance in addressing the challenges posed by poor policies in managing agricultural water use, particularly in water-scarce basins. Various modeling systems are available for quantifying crop actual evapotranspiration (ETa) and biomass needed for measuring the economic output obtained from each unit of irrigation water utilized. The difference in ETa and biomass estimates between the modeling systems could translate into a difference in EIWP outcomes, which influences the basin-wide irrigation water management. In this paper we examine the influence of selecting different ETa and biomass models, particularly the hybrid single-source energy balance HSEB, the Global Field-Scale Crop Yield and ET Mapper in Google Earth Engine GYMEE, and FAO's WaPOR V2, on evaluating EIWP on a basin-wide level. The method includes combining remote sensing and economic data to compare variability in ETa, biomass, and EIWP values derived from HSEB, GYMEE, and WaPOR. The approach is demonstrated with field survey data from the upper hydrologic unit of Lebanon's largest catchment, the Litani River Basin, in its three productive districts Baalbak, Zahleh, and West Bekaa for the year 2021. Field-scale mean monthly ETa and biomass estimates for all crops, obtained from both models, are very comparable. On a district level, the results reveal a reasonable model agreement for the four crops in the estimation of ETa with moderate to strong correlation ( $0.75 < r < 0.95$ ). WaPOR consistently produces slightly higher mean ETa values for potato, wheat, and table grapes when compared to HSEB. Both models reasonably agree when estimating biomass for the four crops with high correlation ( $r > 0.9$ ). Contrary to the ETa results, the GYMEE model consistently estimates slightly higher mean biomass values for all crops compared to WaPOR. The EIWP values produced by both models consistently indicate that potato holds the highest EIWP across all districts, followed by onion, table grapes, and wheat. The mean district HSEB-GYMEE model derived EIWPs are slightly higher than those derived from the WaPOR model for most crops. For EIWP obtained from HSEB-GYMEE, mean EIWP for potato is 12 times higher than that of wheat. As for that obtained from WaPOR, mean EIWP for potato is 10 times higher than that of wheat. The paper establishes a basis for future research on the application of remote sensing models in addressing water-stressed and socioeconomically challenged basins, with the potential to inform strategic irrigation management decisions based on model selection.

## TABLE OF CONTENTS

ACKNOWLEDGEMENTS .....	1
ABSTRACT .....	2
ILLUSTRATIONS .....	5
TABLES .....	6
ABBREVIATIONS .....	7
INTRODUCTION .....	8
1.1. Economic Irrigation Water Productivity for Global Water and Food Challenges	8
1.2. Economic Irrigation Water Productivity: A Key Indicator for Informed Policymaking in Agricultural Water Management .....	9
1.3. Remote Sensing Based Models for EIWP-Informed Policymaking.....	13
METHODS .....	16
2.1. Background to the Case Study: Litani River Basin (LRB).....	16
2.2. Data.....	19
2.2.1. Estimation of Actual Evapotranspiration and Irrigation Water Applied: HSEB and FAO WaPOR .....	20
2.2.2. Biomass and Yield Estimation: GYMEE and FAO WaPOR .....	23
2.2.3. Economic Irrigation Water Productivity (EIWP) and Economic Data.....	31
2.2.4. Statistical Indicators.....	32
RESULTS .....	34
3.1. Remote Sensing-Derived Data Results.....	34

3.1.1. Daily Reference ET of FAO WAPOR, HSEB, and Experimental Field.....	34
3.1.2. Monthly and Seasonal Actual ET and Biomass Estimates of FAO WaPOR and HSEB-GYMEE.....	35
3.1.3. Seasonal Biomass Estimation by WaPOR and GYMEE Models and District- Wise Assessment .....	37
3.1.4. Seasonal Actual ET Estimation by WaPOR and HSEB Models and District- Wise Assessment .....	41
3.2. Economic Data Results.....	43
3.3. Effect of Model Selection on EIWP Results .....	45
<b>DISCUSSION.....</b>	<b>47</b>
4.1. Economic Irrigation Water Productivity Analysis.....	47
4.2. Potential Sources of Modeled Biomass and ET Differences.....	48
4.2.1. Beyond Reference Evapotranspiration .....	48
4.2.2. Environmental Stressors of the Models' Biomass and ET Equations .....	49
<b>CONCLUSION .....</b>	<b>52</b>
<b>APPENDIX 1 .....</b>	<b>54</b>
<b>APPENDIX 2 .....</b>	<b>67</b>
<b>REFERENCES .....</b>	<b>68</b>

# ILLUSTRATIONS

## Figure

1. Geographic location of the study area across the districts of Baalbak, Zahleh, and West Bekaa within the Upper Litani River Basin in Lebanon. .... 17
2. Workflow for the estimation of Economic Irrigation Water Productivity from the three models HSEB, GYMEE, and WaPOR adapted from the methodology of FAO and World Bank (2022). .... 19
3. Start of Season (SOS) and End of Season (EOS) dates and irrigation system type and efficiency for potato, wheat, onion, and table grapes after Jaafar et al. (2016). 23
4. Temporal comparison of Reference Evapotranspiration (ET<sub>ref</sub>) estimates of HSEB and GYMEE models and the measured records at AREC site in Bekaa, Lebanon over the course of 2021..... 35
5. a) Box plots showing monthly actual evapotranspiration (mm) and biomass (Mt/ha) estimates of FAO WaPOR and GYMEE models for all crops; b) Box plots showing actual evapotranspiration (mm/season) and biomass (Mt/ha/season) estimates of both models for onion, potato, table grapes, and wheat during the 2021 growing season in the study area within the Litani River Basin in Lebanon. .... 37
6. (a) Scatterplots comparing modeled biomass estimates; (b) Scatterplots inter-comparing district-disaggregated modeled biomass derived from GYMEE and FAO WaPOR for onion, potato, table grapes, and wheat in the three producing districts Baalbak, West Bekaa, and Zahleh during 2021 growing season in the study area within the Litani River Basin in Lebanon. .... 39
7. Bar charts comparing crop yields of onion, potato, table grapes, and wheat using GYMEE and WaPOR models across three producing districts Baalbak, West Bekaa, and Zahleh during 2021 growing season in the study area within the Litani River Basin in Lebanon. .... 41
8. (a) Scatterplots comparing modeled mean actual Evapotranspiration estimates; (b) Scatterplots comparing modeled district-disaggregated actual Evapotranspiration estimates - derived from HSEB and FAO WaPOR for onion, potato, table grapes, and wheat during 2021 growing season in the study area within the Litani River Basin in Lebanon. .... 42
9. Bar charts comparing actual evapotranspiration of onion, potato, table grapes, and wheat using HSEB and WaPOR models across three producing districts Baalbak, West Bekaa, and Zahleh during 2021 growing season in the study area within the Litani River Basin in Lebanon..... 43
10. Records of mean EIWP (\$/m<sup>3</sup>) values per crop across the three producing districts in the Litani River Basin in Lebanon..... 46

## TABLES

### Table

1. Literature review on definitions of Economic Irrigation Water Productivity (EIWP) for agricultural water management and policy. ....	12
2. General characteristics of the remote sensing-based ET modeling systems used in this study: HSEB (Jaafar et al., 2022) and FAO WaPOR. ....	21
3. User-defined crop-specific parameters for yield estimation of potato, wheat, onion, and table grapes using WaPOR data components. ....	30
4. District-scale cost of production and net revenues derived from FAO WaPOR and HSEB-GYMEE models for selected crops in the producing districts in 2021. ....	45

## ABBREVIATIONS

ET	Evapotranspiration
HSEB	Hybrid Single-Source Energy Balance
WaPOR	Water Productivity Open-access portal Global Field-Scale Crop Yield and ET Mapper in Google Earth
GYMEE	Engine
FAO	Food and Agriculture Organization
EIWP	Economic Irrigation Water Productivity
LUE	Light Use Efficiency
ETa	Actual Evapotranspiration
SOS	Start of Season
EOS	End of Season
HI	Harvest Index
MC	Moisture Content
CWP	Crop Water Productivity
VIIRS	Visible Infrared Imaging Radiometer Suite ECOSystem Spaceborne Thermal Radiometer Experiment on
ECOSTRESS	Space Station
SR	Surface Reflectance
LST	Land Surface Temperature
TIR	Thermal Infrared
GEE	Google Earth Engine
LRB	Litani River Basin
AETI	Actual Evapotranspiration and Interception
Etref	Reference Evapotranspiration
NPP	Net Primary Production
APAR	Fraction of Absorbed Photosynthetically Active Radiation
NDVI	Normalized Difference Vegetation Index
PAR	Photosynthetically Active Radiation
LUEmax	Maximum Light Use Efficiency
VS	Vapor Stress
TS	Temperature Stress
VPD	Vapor Pressure Deficit
SM	Soil Moisture Stress
fPAR	Fraction of Photosynthetically Active Radiation
DMP	Above-ground Dry Matter Production
AGB	Above-Ground Biomass
AREC	Agricultural Research and Education Center
ECMWF	European Centre for Medium-Range Weather Forecasts
MERRA	Modern-Era Retrospective analysis for Research and Applications

# CHAPTER 1

## INTRODUCTION

### **1.1. Economic Irrigation Water Productivity for Global Water and Food Challenges**

Water plays a decisive role in food production. As global water resources continue to decline, there is a greater focus on maximizing the economic output obtained from each unit of irrigation water utilized, known as Economic Irrigation Water Productivity (EIWP), rather than the output obtained from each unit of land (yield) (FAO & World Bank, 2022). As water demands are contingent on yield levels and considering that blue water consumption directly impacts production costs, a farmer might regard economic irrigation productivity as a fitting factor for guiding decisions in irrigation water management (Schmitz et al., 2013; Zisopoulou, Zisopoulos, & Panagoulia, 2022). Crop actual evapotranspiration (ET<sub>a</sub>) and biomass are factored in the evaluation of EIWP, hence the selection of different remote sensing-based ET<sub>a</sub> and biomass models influences the basin-wide assessment of EIWP. The methodological approach adopted by each model becomes a critical determinant in this evaluation process. Potentially, this selection could have an impact on decision-making processes regarding policies and investments in semi-arid regions and water-scarce basins.

Irrigated lands produce much of the world's food and fiber (Foley, Thenkabail, Aneece, Teluguntla, & Oliphant, 2020). While natural rainfall alone would only be sufficient for rainfed crop production, irrigation water is a critical resource that enables the increase of yields and the production of agricultural commodities. Crop production is sparked by the liberalization of global markets, even in basins that are water-scarce, overlooking water availability (Hellegers, Soppe, Perry, & Bastiaanssen, 2010). This

emphasizes the necessity of estimating irrigation water productivity in economic terms. In rainfed crop cultivation, farmers can only grow their crops during the growing season every year due to rainfall reliance, making them highly vulnerable to recurring droughts and flooding under climate change, hence provoking socioeconomic risks (Tubiello et al., 2008). Irrigation is used largely to produce most of the world's supply of crops, while accounting for a significant share of groundwater withdrawals (70%) (Fitton et al., 2019). In applications of agricultural water management and crop yields, accurate and near-daily ET estimates, which constitute a considerable portion of the surface water balance following precipitation, hold essential significance (Arnold, Srinivasan, Muttiah, & Allen, 1999).

## **1.2. Economic Irrigation Water Productivity: A Key Indicator for Informed Policymaking in Agricultural Water Management**

Economic Irrigation Water Productivity (EIWP), a key indicator for informing policymaking in improving irrigation water management, factors in crop yields and irrigation practices observed across different farms and over varying years. Major undertakings aimed at enhancing agricultural water management primarily focus on augmenting the productivity of crops in relation to the amount of water utilized, commonly referred to as Crop Water Productivity (CWP) (Foley et al., 2020; Kang et al., 2017; Molden et al., 2007; Safi, Karimi, Mul, Chukalla, & De Fraiture, 2022; Zwart & Bastiaanssen, 2004). However, particularly in arid and semi-arid regions, water consumption has a significant impact on economic growth, hereafter underscoring the promotion of EIWP as a key assessment tool in agricultural water use (Bashe, Alamirew, & Dejen, 2022). The concept of EIWP plays a central role in recent agricultural water policy interest, particularly in the valuation of irrigation water and

determining cropping priorities. When utilizing performance indicators, notable uncertainties can affect the accuracy of these metrics, including the definition of profit and irrigation water volume.

Scholarly sources report on several definitions of EIWP, of which certain studies integrate remotely sensed ET and crop yields with economic analysis (Table 1).

Droogers, Malik, Kroes, Bastiaanssen, and Van Dam (2003) integrate remote sensing at regional and field scales with four terms of economic water productivity to develop modeling approaches that explore future scenarios of increasing water productivity. The literature indicates that Molden et al. (2007) define water productivity in economic terms as the value derived per unit of water used. Biradar et al. (2008) develop methods for water productivity mapping of irrigated areas on a river basin scale using remote sensing and field-plot data at several spatial, spectral, and radiometric resolutions, and delineate areas of high and low EIWP. A key contribution of Hellegers et al. (2010) is defining EIWP as the net economic benefits per unit of water consumed (USD/m<sup>3</sup>), in other words, the net water return to the producer, also first termed in 2005 as the 'value of water' by Young and Loomis (2014). The net economic benefit is the result of multiplying beneficial biomass by the market price, subtracting the financial production costs (excluding water). According to Nouri et al. (2020), economic irrigation water productivity is determined by dividing the output's value at the farm gate by evapotranspiration. Santos, Lorite, Tasumi, Allen, and Fereres (2010) and Adeboye, Schultz, Adekalu, and Prasad (2015) consider irrigation water applied in the definition of irrigation water productivity rather than solely ET values as cited by previous authors. While these alternative definitions may be simpler to implement than the one employed in this research, they do not account for production costs, and only involve

actual ET instead of irrigation water applied to the field. For crops with substantially varying costs, relying on the gross production value may not be an accurate indicator of differences in return of water. Definitions for measuring the irrigation water volume are adapted from Santos et al. (2010) and Adeboye et al. (2015) which include all on-farm consumptive uses.

Table 1. Literature review on definitions of Economic Irrigation Water Productivity (EIWP) for agricultural water management and policy.

Authors	Case Study	Remote Sensing	Economic Irrigation Water Productivity
Droogers et al. (2003)	Sirsa district, India	Yes. Landsat-7 ETM and NOAA-16 for derivation of actual ET. SEBAL algorithm for crop yield estimation	Expressed per unit of water of 1) crop transpiration, 2) ET, 3) irrigation, and 4) total water supply
Molden et al. (2007)	n/a	No	Value derived per unit of water used
Biradar et al. (2008)	Syr Darya river basin, Central Asia	Yes. Yield modeling and actual ET; Quickbird, Landsat ETM+, IRS-P6-LISS3, MODIS (MOD09Q1 and MOD09A1)	Average market value of crop defined as the economic value (USD) per unit of water used or actual ET
Hellegers et al. (2010)	Inkomati Basin, South Africa	Yes. Actual ET, beneficial biomass, and CWP using SEBAL algorithm and Landsat, MODIS, and TRMM satellite images	Net production value (beneficial biomass and market price minus variable and fixed production costs) per unit of water consumed (\$/m <sup>3</sup> ), following the Residual Method detailed by Young (2014)
Santos et al. (2010)	Genil–Cabra Irrigation Scheme, Southern Spain	Yes	Increase in value of production due to irrigation per volume of irrigation water applied
Adeboye et al. (2015)	Ile-Ife town, Nigeria	No	Marketable crop yield multiplied by the market price per volume of irrigation water applied
Nouri et al. (2020)	Upper Litani Basin, Lebanon	No	Value of output at farm-gate divided by ET

### **1.3. Remote Sensing Based Models for EIWP-Informed Policymaking**

The opportunities for integrating data obtained from remote sensing based ETa and biomass models with economic data are high and vital for informing decision makers on the design of sensible water policy conducive towards sustainable irrigation water-use by farmers (Biradar et al., 2008; Droogers et al., 2003; Hellegers et al., 2010). In data-poor countries with water-scarce basins, water productivity challenges are serious due to the sparse availability of proper irrigation infrastructure, ground measurements, and water metering technologies. These limitations often hinder the ability to gather information about spatial water use changes occurring at large extents, marking the value of frequent satellite observations (McShane, Driscoll, & Sando, 2017). Remote sensing, which is more suited for mapping spatial and temporal variability, has made it possible to estimate near real-time water productivity, and has emerged as an effective and reproducible technique to complement point-based ET observational methods (Jaafar, Mourad, & Schull, 2022). In a review performed to assess the accuracy of remotely sensed and in-situ water productivity products, Blatchford, Mannaerts, Zeng, Nouri, and Karimi (2019) identified that remote sensing can estimate water productivity within the error range of in-situ methods. Users and managers of water resources have a stake in accurately estimating water use. Over the past few years, several modeling systems were developed for estimating actual evapotranspiration (ETa) at scales useful to water resource managers - agricultural fields and the extent of river basins. Recent efforts (Guzinski & Nieto, 2019) employed a sharpening machine-learning algorithm based on the use of Sentinel-2 and Sentinel-3 satellite images to generate 20m ET. There were also attempts to sharpen thermal data sourced from ECOsystem Spaceborne Thermal Radiometer Experiment on Space

Station (ECOSTRESS) and the Visible Infrared Imaging Radiometer Suite (VIIRS) using the harmonized Landsat and Sentinel-2 Surface Reflectance (SR) data at 30m resolution (Xue et al., 2020). The Food and Agriculture Organization (FAO) Water Productivity Open-access portal (WaPOR) ETLook model, uses the Penman Monteith approach to generate ETa by deriving soil moisture from Land Surface Temperature (LST) inputs (FAO, 2020). Detailed methodology of the ETLook algorithm is described in (Bastiaanssen, Cheema, Immerzeel, Miltenburg, & Pelgrum, 2012). Jaafar et al. (2022) expanded on previous efforts and developed a Hybrid Surface Energy Balance ‘HSEB’, a field-scale ET model with validated global operational capabilities, and maximized spatiotemporal resolution, by sharpening Thermal Infrared (TIR) inputs with harmonized SR data from Sentinel-2, Landsat, and digital elevation data.

In addition to ET models, EIWP also relies on remote sensing-based biomass models to obtain crop yields. A significant body of literature proposes that the radiation or light use efficiency (LUE)-based biomass model, as introduced by Monteith (1972), holds substantial promise for accurately estimating crop yield when integrated with satellite data. However, this method relies on the use of medium-resolution data, which may pose limitations when attempting to apply it to small fields. The WaPOR V2 biomass methodology is based on the C-Fix Model described in (Veroustraete, Sabbe, & Eerens, 2002). Recent efforts (Jaafar & Mourad, 2021) developed the Global Yield and Evaporation Mapper in Earth Engine (GYMEE) which is a Google Earth Engine (GEE)-grounded operational remote sensing and evapotranspiration-based light use efficiency model that estimates the global crop yield at 30 m resolution using Landsat satellite imagery, combined with gridded weather data and global soil datasets. The

results of the study suggest that the model is of high value for estimating the yield of wheat, potato, and corn in Mediterranean, semi-arid, and tropical climates.

This research examines the influence of selecting different ETa and biomass models, particularly HSEB, GYMEE, and FAO's WaPOR V2, on evaluating EIWP on a basin-wide level. The difference in ET and biomass estimates between the modeling systems could translate into a difference in economic irrigation water productivity outcomes, which provides reference for decision making in on-farm irrigation. We build upon the methodology developed by FAO and World Bank (2022). The usefulness of combining remote sensing and economic data to assess variability in EIWP is demonstrated with field survey data from the Upper Litani River Basin in Lebanon in the three productive districts Baalbak, Zahleh, and West Bekaa. The aim is to gain a deeper understanding of the disparities between model results and the variations observed across different zones within the basin. During a science-policy stakeholder workshop conducted in Beirut in April 2023, it was agreed that some strategies which are effective in one zone of the Upper Litani Basin may not necessarily be applicable to other zones within the same basin. Rather, a more nuanced approach may be required, where strategies are tailored to the specific needs and characteristics of each zone to maximize their effectiveness. While the current study is based on potato, wheat, table grapes, and onion, the same framework can be expanded to other crops

## CHAPTER 2

### METHODS

#### **2.1. Background to the Case Study: Litani River Basin (LRB)**

The Litani River Basin (LRB) is experiencing water shortages and is representative of many other river basins in the Mediterranean region. Lebanon ranks among the five most water-stressed countries due to the significant demand placed on irrigated agriculture, paired with other contributing drivers, according to Kuzma, Saccoccia, and Chertock (2023). The LRB, the country's largest catchment with a total area of 217,600 ha (20% of Lebanon's total area), consists of two main hydrologic units: the Upper Litani Basin and the Lower Litani Basin. These two units are interconnected in the central part of the basin at the Qaraoun reservoir. The pilot study area for the implementation of the FAO WaPOR tool lies within the Upper Litani River Basin, encompassing the fertile Bekaa agricultural plain. Population increase is the primary driving force modifying demands on the basin's available water resources, where inhabitants live under water stress (Jaafar, Ahmad, Holtmeier, & King-Okumu, 2020). The basin is of major concern to local stakeholders and river basin planners as more than 45,000 ha are devoted to irrigated agriculture in the 180,000 ha Upper Litani Basin (Jaafar et al., 2016), and more than 320 million cubic meters of water is estimated to be pumped from groundwater in this basin (Jaafar & Ahmad, 2020). About 60% of water withdrawals come from irrigated agriculture, most of which are met through groundwater extractions, while currently groundwater resources in the LRB are depleted by around 57.5 million cubic meters per year (Jaafar et al., 2016).

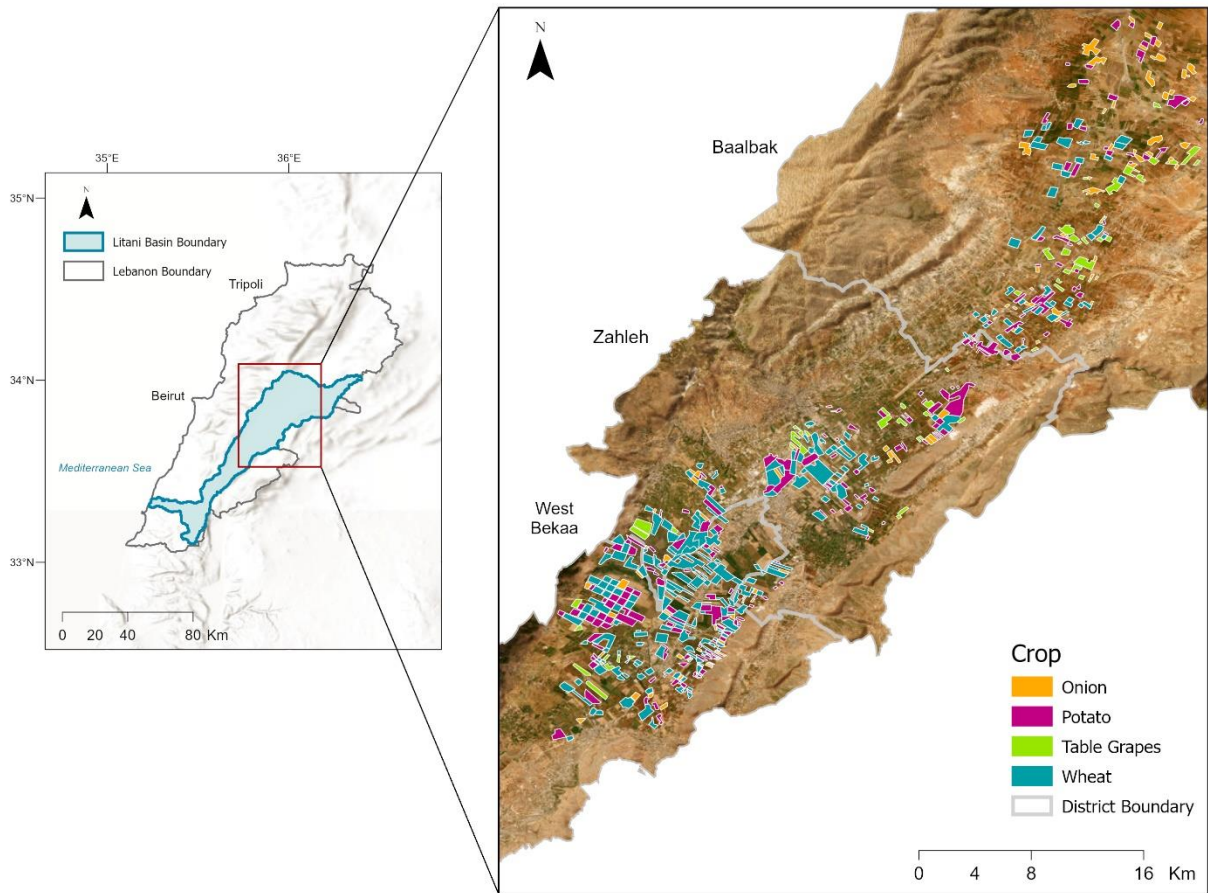


Figure 1. Geographic location of the study area across the districts of Baalbak, Zahleh, and West Bekaa within the Upper Litani River Basin in Lebanon.

On top of agricultural water demand, the river supplies water to over a million inhabitants with conflicting water uses including domestic, municipal, and hydropower, while cross-bordering three administrative areas: South Lebanon, Baalbak-Hermel, and Bekaa, and joining the inner and the coastal zones of Lebanon. Most of the domestic and industrial water in the basin is left untreated, with high levels of pollution resulting in non-recoverable flow of about 469.5 million cubic meters per year (Jaafar et al., 2016), threatening public health and ecosystem functions. The Litani River is a key component in Lebanon's socioeconomic growth, as it is a central hub of agricultural and human activities, with agriculture in the Bekaa valley being the largest water consumer

in the basin. The Bekaa agricultural plain, the nation's breadbasket, is nourished by the 176 km Litani river, which irrigates thousands of hectares of agricultural land including potato, wheat, onion, and table grapes (Jaafar et al., 2016).

The LRB is recharged by local rainfall episodes limited to 90 to 100 days between October and April with an average annual precipitation of 630 mm, as well as by snowmelt from snowfall that occurs at elevations above 1,200 m for 25-30 days per year. The river flow is hence characterized by a seasonal pattern and a significant interannual variability. Abrupt dissimilarities are prevalent in temperatures across the catchment of the LRB due to its varied topography with a mean monthly temperature of 21.5°C. The Mediterranean climate in the Bekaa is marked by hot, dry summers and wet winters, placing a high demand on pumping water for irrigating agriculture, which exceeds the annual recharge, likewise other developing countries – Libya, Saudi Arabia, Yemen, and Egypt – where it is estimated that the annual amount of water used for irrigation exceeds their renewable water resources (Alexandratos & Bruinsma, 2012). To sustain crop yields during this climate, farmers in the LRB irrigate crops from May to October, which is the main irrigation season in the basin (Jaafar et al., 2020).

Of particular interest to our study is leveraging accurate crop mapping of the Bekaa agricultural plain for the derivation of reliable ET, biomass, and EIWP values. The crop maps generated by WaPOR automatically differentiate between irrigated and rainfed pixels. However, this classification may not always be accurate, particularly for crops that receive supplementary irrigation such as wheat (FAO & World Bank, 2022). The study area covers agricultural fields surveyed during the 2021 summer season in the months of May to August, across the three producing districts: Zahleh, Baalbak, and

West Bekaa. The 17-day field survey maps 30 crops in the Bekaa plain, of which the major crops, namely potato, wheat, onion, and table grapes, were involved in this study.

## 2.2. Data

Figure 2 provides a schematic representation of the framework for estimating EIWP from the different ET and biomass models (HSEB, GYMEE, and WaPOR) for the studied crops during the 2021 growing season in the study area within the Litani River Basin in Lebanon. The illustration is adapted from FAO and World Bank (2022). First, field-scale actual ET and biomass estimates from the models are derived and compared. Second, a) actual ET figures from both models are used to calculate the irrigation water volume component of EIWP by deriving water applied by farmers at the field scale based on ET from rainfall, while accounting for the irrigation system efficiency in the analysis; b) the biomass values are used to estimate crop yields which are needed for the profit component of EIWP. Third, field-scale EIWP values from both models are derived and analyzed.

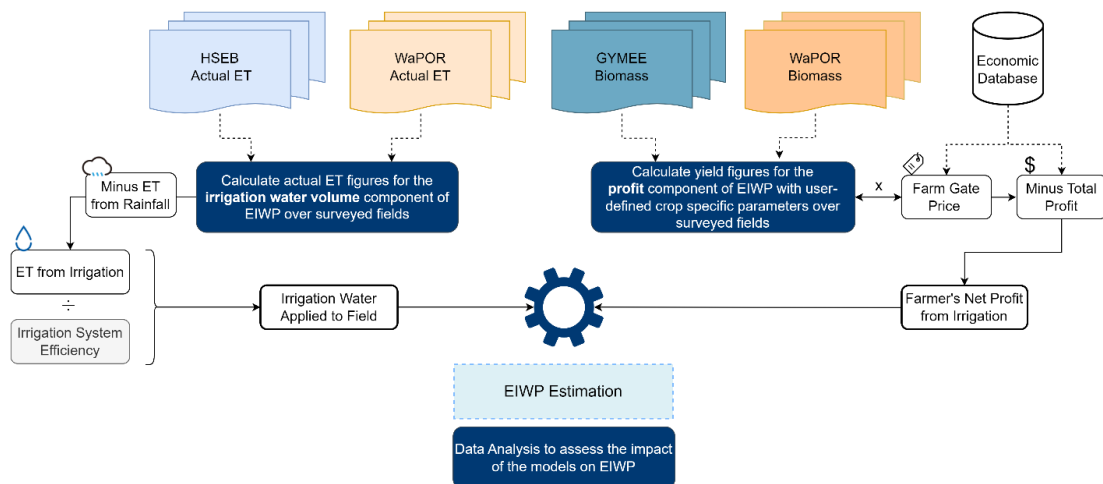


Figure 2. Workflow for the estimation of Economic Irrigation Water Productivity from the three models HSEB, GYMEE, and WaPOR adapted from the methodology of FAO and World Bank (2022).

### ***2.2.1. Estimation of Actual Evapotranspiration and Irrigation Water Applied: HSEB and FAO WaPOR***

We use actual Evapotranspiration (ETa) to quantify agricultural water consumption. A significant divergence between WaPOR and HSEB models is whether the vegetation and soil components are treated independently as in the WaPOR approach, or as a combined composite as in the hybrid single-source energy balance model, HSEB, which treats the land surface as a bulk source of water vapor and heat (Jaafar et al., 2022). The WaPOR modeling system involves the sum of all three parameters: the soil evaporation (E), canopy transpiration (T), and evaporation from rainfall intercepted by leaves (I), where the value of each pixel represents ETa in each month. HSEB generates a 5-day ET product for any land location at a 30 m spatial resolution, which are further aggregated to weekly and monthly time steps, by combining MODIS and VIIRS LST, Landsat thermal bands, and the harmonized surface reflectance of Sentinel-2 and Landsat. WaPOR on the other hand is available at a 30 m resolution at three temporal extents: dekadal, monthly, and annual. Table 2 summarizes the general characteristics of the two remote sensing-based ET modeling systems HSEB and FAO WaPOR. We use HSEB to derive agricultural water use values because it utilizes finer resolution imagery that is more suitable to estimate ETa in the heterogeneous landscape of the Litani River Basin study area than models with coarser resolution.

Table 2. General characteristics of the remote sensing-based ET modeling systems used in this study: HSEB (Jaafar et al., 2022) and FAO WaPOR.

	<b>HSEB</b>	<b>WaPOR</b>
Model	Single-source energy balance	ETLook (Bastiaanssen et al., 2012)
Parameters		
Temporal Resolution	Daily, weekly, monthly	Dekadal, monthly, annual
Spatial Resolution	10-20m and 30m	Between 30m and 250m
Spatial Coverage	Global	Africa and Near East
Operational Environment	Google Earth Engine	

We used sub-national 30m spatial resolution Actual Evapotranspiration and Interception (AETI, hereafter ETa for consistency) datasets derived from WaPOR V2.1 on a monthly temporal resolution over the Bekaa, Lebanon, in conjunction with the surveyed crop-type mapping to generate monthly and seasonal actual ET quantities of each crop at the field scale. ETa raster data were scaled as per WaPOR conversion factor, and monthly sum ETa was calculated for each crop following the local farmer's agricultural practices and crop calendar. Zonal statistics were performed in GEE over the fields to derive the mean monthly ETa of each crop. We summarized mean crop ETa over the growing season (mm) per district (Baalbak, Zahleh, and West Bekaa) by accumulating monthly ETa values (mm) from Start of Season (SOS) to End of Season (EOS).

For the HSEB-modeled ETa, we calculated the average ETa for each scene captured by both Landsat 7 and 8 satellites over individual fields during the twelve months of 2021. This data was obtained using Google Earth Engine (GEE). Subsequently, we aggregated this data to obtain monthly and seasonal ETa values for each field. To compute the monthly ETa, we first determined the average ETa across all the scenes available for a particular month. This average was multiplied by the number

of days in that specific month to obtain the total ETa for that month. These monthly ETa values were then summed up to obtain the seasonal ETa for each field.

Additionally, we undertook a comparison of the reference evapotranspiration (ETref) derived from both the HSEB and the WaPOR ETref models over the Bekaa, as well as a comparison of the seasonal ETa values obtained from both models, encompassing all fields under consideration. We seek to identify whether the discrepancies arise from variations in the computation of ETref between the HSEB model utilized by GYMEE and the method employed by WaPOR, or if they stem from differences in the subsequent conversion from ETref to ETa. The objective of this comparison was to evaluate the disparities in output between these two models and to determine if significant variations exist in the estimation of actual evapotranspiration across diverse districts within the basin.

We derived irrigation ET per crop by summing ETa values derived from both models during the summer months when irrigation was applied. In this study, there is a critical distinction between irrigation water applied by the farmer and water consumed by the crop. Irrigation water applied to the field is the preferred metric since it enables a straightforward comparison between the irrigation water net return and the price (FAO & World Bank, 2022). We quantified water applied by farmers at the field scale (1) based on crop seasonal ETa and ET from rainfall, while accounting for the irrigation system efficiency in the analysis (Figure 3). Irrigation system efficiency is the fraction of irrigation water applied that is beneficially consumed by the crop and can be increased by modern irrigation technologies (Perry, 2007). Irrigation system efficiencies and types in the Bekaa were adapted from Jaafar et al. (2016).

$$\text{Seasonal Irrigation Water Applied to Field} = \frac{\text{Irrigation } ET_{\text{seasonal}}}{\text{Irrigation System Efficiency}} \quad (1)$$

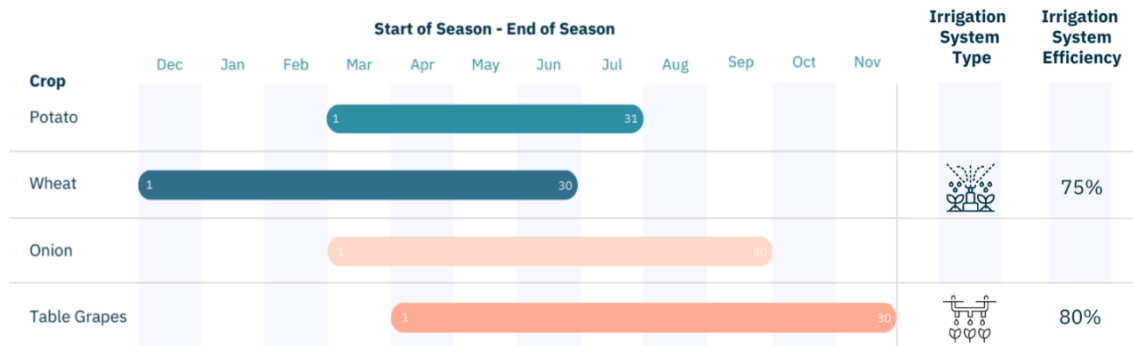


Figure 3. Start of Season (SOS) and End of Season (EOS) dates and irrigation system type and efficiency for potato, wheat, onion, and table grapes after Jaafar et al. (2016).

## 2.2.2. Biomass and Yield Estimation: GYMEE and FAO WaPOR

### 2.2.2.1. Biomass Comparison and Estimation

Familiarity with the method of computing variables within various biomass models is essential for assessing Net Primary Production (NPP), which is a key component in biomass models (Running, Nemani, Glassy, & Thornton, 1999), particularly in semi-arid regions and water-scarce basins. On both global and regional levels, earth observation-based calculations of fraction of absorbed photosynthetically active radiation (APAR) as well as environmental stressors play a crucial role in evaluating yield estimates.

#### 2.2.2.1.1. Comparative Analysis of GYMEE and WaPOR Biomass Models

Ongoing research has aimed to establish more physically grounded correlations between vegetation growth and the Normalized Difference Vegetation Index (NDVI) by employing parametric models. These models generally stem from the concept of Light Use Efficiency (LUE) proposed by Monteith (1972), seeking to delineate light

absorption by plant canopies through a relation between NDVI and fraction of Absorbed Photosynthetically Active Radiation (APAR) (Goward & Huemmrich, 1992; Hanan, Prince, & Bégué, 1995). APAR denotes the fraction of sunlight absorbed by leaves within the 0.4–0.7  $\mu\text{m}$  spectrum and consequently reflects a canopy's energy absorption capacity (Fensholt, Sandholt, & Rasmussen, 2004). APAR retains its expression as a ratio but can be transformed into absorbed photosynthetically active radiation, often measured in  $\text{MJ}/\text{m}^2$ , by multiplying the fPAR ratio with incident Photosynthetically Active Radiation (PAR). The utilization of the LUE principle for NPP modeling hinges upon a robust correlation between the biophysical variables APAR and NDVI. A multitude of researchers have examined this relationship, with consensus indicating a compelling linkage between APAR and NDVI (Myneni et al., 2002). Empirical evidence derived from satellite observations suggests that the relationship between NDVI and APAR is either linear or approximately linear for green vegetation (Prince & Goward, 1995; Ruimy, Saugier, & Dedieu, 1994), a conclusion further supported by radiative transfer models (Goward & Huemmrich, 1992; Myneni & Williams, 1994). Significantly for our investigation, the GYMEE model integrates an equation for fPAR expressed as  $1.257 \times \text{NDVI} - 0.161$  (Jaafar & Mourad, 2021), whereas the WaPOR V2 model employs a fPAR equation of  $0.8642 \times \text{NDVI} - 0.0814$ , as derived from the work of (Veroustraete et al., 2002). For the sake of our comparative analysis, the fPAR equation from WaPOR V2 was employed consistently across both models.

We followed the processing chain of each biomass model (GYMEE and WaPOR V2 - level 3) and dissected the variances between their equations. Our analysis delved into these equations and how they might affect the biomass values generated by each model. This, in turn, has significant implications for the decision-making process

surrounding crop yields, hence impacting EIWP. As outlined in Table 1A in Appendix 1, we broke down the GYMEE and WaPOR V2 biomass equations, elucidating the specific data components involved. This encompasses fundamental elements crucial to biomass derivation, as well as the comprehensive consideration of environmental stressors.

#### 2.2.2.1.2. Parameter Equation Differences in Net Primary Production

Net Primary Production (NPP) represents the conversion of carbon dioxide into biomass through photosynthesis and is a crucial feature of an ecosystem (FAO, 2020; Running et al., 1999). In the WaPOR V2 biomass model, the NPP value for each pixel corresponds to the average daily NPP for that specific dekad (gC/m<sup>2</sup>/day). The determination of NPP involves six key factors, including daily weather data (Tmin/Tmax) and solar radiation, dekadal inputs from APAR, soil moisture stress, as well as seasonal inputs from land cover-specific light use efficiencies (Swinnen, Van Hoolst, & Toté, 2019) and CO<sub>2</sub> (for more details on the methodology, reader can refer to FAO (2020) and the C-Fix model of Veroustraete et al. (2002)). In the GYMEE model, NPP is calculated as a product of APAR, light use efficiency (LUE), and the impact of the environmental stressors affecting biomass production.

Comparing the two NPP equations of WaPOR V2 (5) and GYMEE (6), we observe that the LUEmax values are different for the two models (2.5 g/MJ for GYMEE and 2.7 g/MJ for WaPOR V2, which is to be updated to 2.49 g/MJ in the upcoming WaPOR V3 (FAO, 2023). LUEmax specifically refers to the maximum efficiency at which plants convert absorbed light energy into biomass through photosynthesis achievable under optimal conditions. However, the relationship between LUEmax and

biomass is influenced by various factors such as environmental conditions, which may drive biomass differences. We also observe that the GYMEE model includes additional stress factors, Vapor Stress (VS) and Temperature Stress (TS). The HSEB-GYMEE model accounts for plant temperature constraint (TS) in its actual ET model based on the relationship between temperature stress and Jarvis coefficient (FRAME, 2020; Jaafar & Mourad, 2021). Additionally, the 0.63 factor in the WaPOR equation captures the fraction kept after autotrophic respiration ( $\epsilon AR$ ) effect and the normalized CO<sub>2</sub> fertilization ( $\epsilon CO_2$ ) effect on biomass (Veroustraete et al., 2002). Within the GYMEE model, the Vapor Pressure Deficit (VPD) is regarded as a significant factor affecting the water and carbon requirements of crops (Jaafar & Mourad, 2021). We additionally note that the coefficient 0.864 within the GYMEE equation serves unit conversion. This conversion factor accommodates the shift from W/m<sup>2</sup> to MJ/m<sup>2</sup>/day and compensates for alterations in area units from square meters to hectares. Both models incorporate Soil Moisture Stress (SM) as a reduction factor to account for lowered water availability. GYMEE captures SM by characterizing anomalies in the actual-to-potential 24-hour transpiration ratio ( $T_{act24}/T_{pot24}$ ) through the energy balance with the standardized American Society of Civil Engineers (ASCE, 1996) – Penman–Monteith equation, as described by Jaafar and Mourad (2021). On the other hand, WaPOR builds upon the trapezoid method introduced by Yang et al. (2015), an advancement over Carlson's Triangle method from (Carlson, 2007) (for details on the SM equations per model, reader can refer to Table 1A in Appendix 1).

$$WaPOR\ NPP = NPP_{max} \times fPAR \times SM \times \epsilon LUE \quad (2)$$

where:

**NPP:** Net Primary Production [gC/m<sup>2</sup>]

**NPP<sub>max</sub>:** Maximum Net Primary Production [gC/m<sup>2</sup>]

**fPAR:** Fraction of Photosynthetically Active Radiation [-] equals to  $0.8642 \times NDVI - 0.0814$  and which is being updated to  $1.257 \times NDVI - 0.161$  in WaPOR V3 similar to that of GYMEE.

**SM:** Soil Moisture Stress reduction factor [-]

**εLUE:** Light use efficiency at optimum conditions [g/MJ], taken as 2.7 g/MJ in WaPOR V2 and as 2.49 g/MJ in WaPOR V3

$$NPP_{max} = \epsilon T \times \epsilon CO2 \times \epsilon AR \times PAR_{daily} \times S_c \quad (3)$$

where:

**εT:** Normalized temperature effect [-]. 1 (Values of εT range from 0 to 1. In C-fix Model at 25°C, εT is around 1)

**εCO2:** Normalized CO2 fertilization effect [-]

**εAR:** Fraction kept after autotrophic respiration equals to 0.5 [-]

**PAR<sub>daily</sub>:** Photosynthetically Active Radiation [W/m<sup>2</sup>] equals to  $0.48 \times R_s$ ;

where  $R_s$  is the incoming shortwave radiation [W/m<sup>2</sup>]

**S<sub>c</sub>:** conversion factor from DM to C [gC/gDM]  $1\ gC/m^2/day\ (NPP) = 22.222\ kgDM/ha/day\ (DMP)$ .

By substituting the equation for NPP<sub>max</sub> (3) into the equation for NPP (2), we can derive the resulting equation (5) (reader can refer to Table 1A in Appendix 1):

$$WaPOR\ NPP = \epsilon T \times \epsilon CO2 \times \epsilon AR \times PAR_{daily} \times S_c \times fPAR \times SM \times \epsilon LUE \quad (4)$$

With  $DMP = NPP \times 22.222$

where:

*DMP* is the Above-Ground Dry Matter Production (DMP) [kg/ha]

*APAR*: Fraction of Absorbed Photosynthetically Active Radiation [W/m<sup>2</sup>]

$$WaPOR\ NPP = APAR \times \epsilon LUE \times SM \times 0.63 \times S_c \quad (5)$$

$$GYMEE\ NPP = APAR \times \epsilon LUE \times SM \times TS \times VS \quad (6)$$

where:

*NPP*: Net Primary Production [g/m<sup>2</sup>/day]

*APAR*: Fraction of Absorbed Photosynthetically Active Radiation [MJ/m<sup>2</sup>/day]

$\epsilon LUE$ : Light use efficiency at optimum conditions [g/MJ], taken as 2.5 g/MJ in

*GYMEE*

*SM*: Soil Moisture Stress reduction factor [-]

*TS*: Temperature Stress [-] according to Stewart (1987) and Stewart (1988) after Jarvis (1976)

*VS*: Vapor Stress [-]

$$APAR = fPAR \times PAR_{daily} \quad (7)$$

where:

*APAR*: Fraction of Absorbed Photosynthetically Active Radiation [MJ/m<sup>2</sup>/day]

*fPAR*: Fraction of Photosynthetically Active Radiation [-] equals to  $1.257 \times NDVI - 0.161$ .

*PAR<sub>daily</sub>*: Photosynthetically Active Radiation [MJ/m<sup>2</sup>/day]

Above-ground Dry Matter Production (DMP) can be used to derive yields during the crop growing season. DMP comparative equations of WaPOR V2 (8) and GYMEE (9) are presented below.

$$DMP_{WaPOR} = APAR \times LUE_{max} \times SM \times 0.63 \quad (8)$$

$$DMP_{GYMEE} = APAR \times LUE_{max} \times SM \times TS \times VS \times 0.864 \quad (9)$$

where:

*DMP: Above-ground Dry Matter Production [kg/ha]*

#### 2.2.2.2. Crop Yield Estimation

Accurate crop yield estimation is important for calculating EIWP values. Yield is defined as the marketable part of the total above ground biomass production (Zwart & Bastiaanssen, 2004). We estimated the yields of potato, wheat, onion, and table grapes in 2021 in the three producing districts using the Global Yield Mapper in Earth Engine (GYMEE) (Jaafar & Mourad, 2021) and FAO WaPOR V2 land data components. The two light-use efficiency-based models rely on the efficiency of the crop to convert the light absorbed or the water transpired into biomass as key parameters for crop yield modeling, unlike other water use efficiency-based models such as AquaCrop (Steduto et al., 2009) and CropSyst (Stockle, Martin, & Campbell, 1994), which rely on crop transpiration as a main measure of yield estimation. We computed the WaPOR-derived and GYMEE-derived agricultural yields of the cropping season over the survey field-boundary map on a district-disaggregated scale with user-defined crop-specific parameters: harvest index and moisture content presented in Table 3. The Harvest Index (HI) is employed to differentiate between harvestable and non-harvestable biomass production fractions and serves as an indicator of the amount of biomass output that contributes to the harvestable fraction of a crop (FAO, 2020), referred to as yield in this study. Moisture Content (MC) denotes the moisture content of plants on a wet weight basis. The C4 factor was set to 1.00, as all crops are C3 crops.

Table 3. User-defined crop-specific parameters for yield estimation of potato, wheat, onion, and table grapes using WaPOR data components.

Crop Type	HI	MC	C4
Potato	0.79	0.79	1
Wheat	0.39	0.15	1
Onions	0.7	0.88	1
Table Grapes	0.31	0.75	1

We calculated the seasonal Above-Ground Biomass (AGBs) (kg/ha/season) using equation (10) for DMP (Dry Matter Production in kg/ha/dekad) for the WaPOR V2 estimates, while we interpolated GYMEE field-scale DMP values to monthly estimates based on satellite overpass values which were obtained from the GEE environment. Crop yields derived from both models are computed using equation (11) to arrive at seasonal estimates.

$$AGB_s = \sum_{i=SOS}^{EOS} DMP_i \times Nd_i \times AOT \quad (10)$$

where:

*AGB<sub>s</sub>*: Seasonal Above-Ground Biomass, defined as sum of the above-ground dry matter produced during the crop growing season [kg/ha/season].

*DMP*: Above-ground Dry Matter Production [kg/ha]

*Nd<sub>i</sub>*: number of days within each dekad, varying between 8 and 11

*AOT*: Fraction between above and total biomass

$$Y = \frac{AGB_s \times HI \times C_4}{(1-MC)} \quad (11)$$

where:

*Y*: Seasonal crop marketable above ground biomass production [kg/ha/season]

*HI*: Dry basis crop Harvest Index

*MC: Wet basis crop Moisture Content*

### **2.2.3. Economic Irrigation Water Productivity (EIWP) and Economic Data**

Economic productivity is an appropriate metric to use for comparing different crops in different locations and is commonly the foundation for arguing in favor of water transfers among different types of uses (e.g., agriculture, farmers, upstream and downstream, sectors) (Adeboye et al., 2015; FAO & World Bank, 2022; Santos et al., 2010). Although economic productivity can be blurred by fluctuations in crop-related market prices, it remains preferable when comparing different crops (Droogers et al., 2003). In the present work, Economic Irrigation Water Productivity (EIWP) is defined as the profit caused by irrigation generated for the producer by the evapotranspiration of one cubic meter of irrigation water applied to the field (12).

$$\text{Economic Irrigation Water Productivity} = \frac{\text{Profit from Irrigated Crop}}{\text{Irrigation Water Applied to Field}} \quad (12)$$

*where:*

*Economic Irrigation Water Productivity (EIWP) in \$/m<sup>3</sup>.*

*Profit for the producer caused by irrigation in \$/ha.*

*Irrigation Water Applied to Field in m<sup>3</sup>/ha.*

Young and Loomis (2014) describes the ‘value of water’ using the basic approach of the residual method, which computes the value of water as a function of the price by quantity of the output, less the prices by quantities of all known inputs, all divided by the quantity of the water applied. This approach is useful when the quantity of water is limited in its availability as an input to agricultural production, as often occurs in water-scarce basins like the Litani River Basin.

To obtain the net profit as termed by Bellù (2013), we subtracted the total cost of production from the total production value (marketable biomass x farm gate price) following the approach employed by most analysts, particularly for assessing policies on the irrigation of agricultural crops (Young & Loomis, 2014). Production costs include costs of operation, fertilizers, pesticides, labor, diesel, land rental, and seeds and cuttings. Economic inputs derived from crop variable costs and farmer's profit (see Appendix 2 for inclusion criteria for economic data) were collected using a desk study strategy for an in-house crop cost economic assessment for potato, wheat, onion, and table grapes, as well as using official national reports and datasheets of the Ministry of Agriculture and the Ministry of Energy and Water. Since remote sensing cannot determine how these costs vary in practice among farmers, the assumption is made that some of the costs associated with production are fixed. Even though it is an oversimplification of reality, the method is transferable, uniformly applied, and easy to correct.

#### ***2.2.4. Statistical Indicators***

Statistical analysis was based on commonly used and complimentary statistical indicators, including correlation coefficient ( $r$ ), Root Mean Square Error (RMSE), mean bias error (MBE), coefficient of determination ( $R^2$ ), and percent relative error (RE%). The correlation coefficient ( $r$ ) shows the trend of the estimates, and values that are close to unity (1) suggest better performance. RMSE measures the difference between the estimated and actual values, indicating a well-performing model if RMSE values are near zero. MBE values above zero denote overestimation, while values below zero signify underestimation.  $R^2$  is commonly used to assess the goodness of fit of a

regression model. RE% is used for reliable prediction, providing a sense of accuracy in terms of percentage deviation. In the equations below, n is the number of data,  $A_i$  and  $P_i$  are the actual and predicted data values.

$$\text{Root Mean Square Error: } RMSE = \sqrt{\frac{\sum_{i=1}^n (A_i - P_i)^2}{n}}$$

$$\text{Mean Bias Error: } MBE = \frac{\sum_{i=1}^n (A_i - P_i)}{n}$$

$$\text{Relative Error: } \%RE = \frac{|Absolute\ Error|}{A} \times 100$$

$$\text{Correlation Coefficient: } r = \frac{\sum_{i=1}^n (A_i - \bar{A})(P_i - \bar{P})}{\sqrt{\sum_{i=1}^n (A_i - \bar{A})^2 \sum_{i=1}^n (P_i - \bar{P})^2}}$$

$$\text{Coefficient of Determination: } R^2 = \frac{\sum_{i=1}^n (A_i - \bar{A})(P_i - \bar{P})}{\sqrt{\sum_{i=1}^n (A_i - \bar{A})^2 \sum_{i=1}^n (P_i - \bar{P})^2}}$$

## CHAPTER 3

### RESULTS

#### **3.1. Remote Sensing-Derived Data Results**

##### ***3.1.1. Daily Reference ET of FAO WAPOR, HSEB, and Experimental Field***

Figure 4 shows a temporal record of the reference evapotranspiration (ET<sub>ref</sub>) values obtained from WaPOR and HSEB models as well as the measured ET<sub>ref</sub> at an experimental field at the American University of Beirut's Agricultural Research and Education Center (AREC) in the Bekaa, Lebanon. The alignment observed in the daily ET<sub>ref</sub> plots from both remote sensing models over the course of 2021 points to a general consistency in their estimations. However, deviations emerge between the models, as well as in comparison to the measured values, particularly peaking during the intense evapotranspiration activity of the summer months. On average, the WaPOR model demonstrates a mean difference that is 17% higher than HSEB and 4.5% higher than the measured values. HSEB diverges more significantly, standing at a 12% lower deviation from the reported yield. Consistently lower ET<sub>ref</sub> values are seen with HSEB in contrast to the reported values and WaPOR estimates throughout the entire year. During the winter months (January to April and October to December), the values from WaPOR and the site station readings slightly intersect.

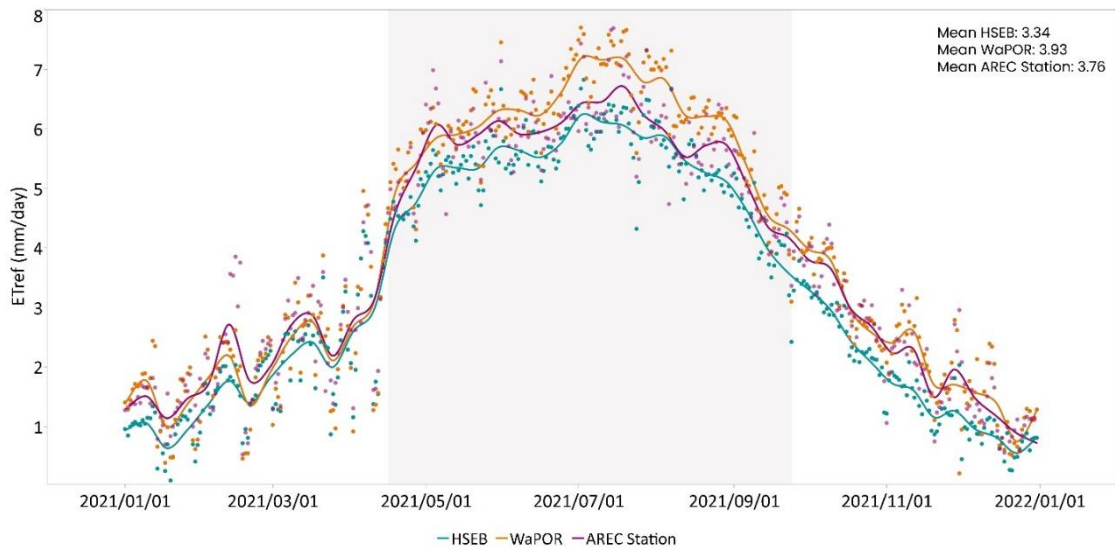


Figure 4. Temporal comparison of Reference Evapotranspiration ( $ET_{ref}$ ) estimates of HSEB and GYMEE models and the measured records at AREC site in Bekaa, Lebanon over the course of 2021.

### ***3.1.2. Monthly and Seasonal Actual ET and Biomass Estimates of FAO WaPOR and HSEB-GYMEE***

Figure 5a shows that the monthly mean  $ET_a$  estimates for all crops, obtained from both models, are very comparable, showcasing values of 105 mm and 101 mm for WaPOR and HSEB, respectively. The biomass values demonstrate a similar level of comparability, with mean estimates of 1.9 t/ha and 2.14 t/ha for WaPOR and GYMEE, respectively.

Figure 5b shows a comparison of seasonal  $ET_a$  and biomass estimation between WaPOR and HSEB-GYMEE models per crop. For potato, table grapes, and wheat, the mean ET values derived from WaPOR tend to be slightly higher than those from the HSEB model (612, 573; 928, 871; and 660, 621) mm/season respectively, whereas the opposite trend is observed for onion (725, 751). Notably, the standard deviation values for ET data, both from WaPOR and HSEB, appear to be within a reasonably comparable range across the different crops. Contrary to the ET results, the GYMEE

model consistently yields moderately higher mean biomass values compared to WaPOR for all crops, onion, potato, table grapes, and wheat (10.9, 13.4; 11, 12.7; 15.7, 17.6; and 12.6, 13.6) Mt/ha/season respectively. Similar to the ETa standard deviation results, the standard deviation values for biomass data also exhibit consistency between the models for each crop. The subtle variations in mean values might be attributed to differences in the underlying algorithms and assumptions of the models. The relatively consistent standard deviation values suggest that the models demonstrate similar levels of variability in their estimates for different crops.

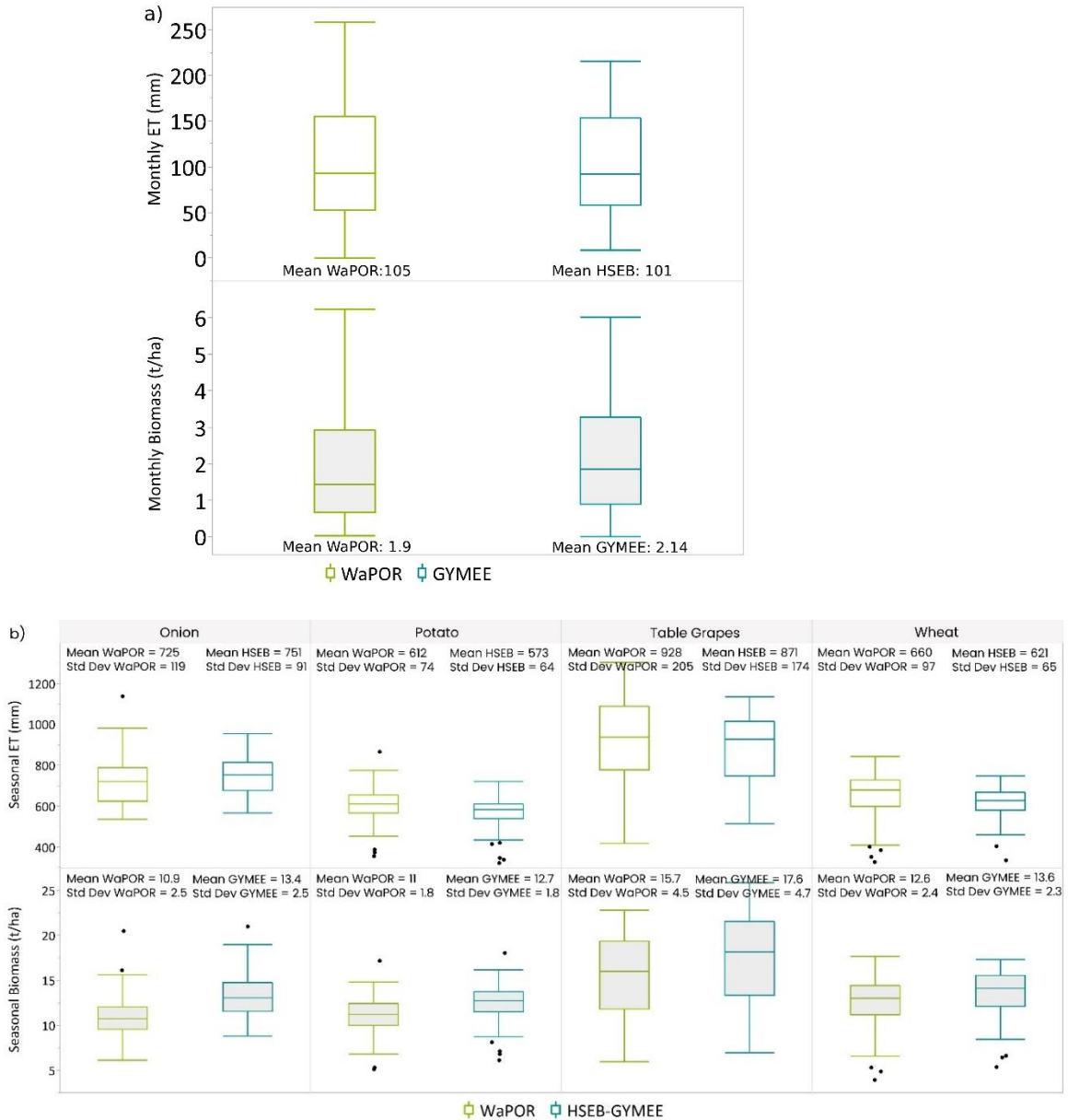


Figure 5. a) Box plots showing monthly actual evapotranspiration (mm) and biomass (Mt/ha) estimates of FAO WaPOR and GYMEE models for all crops; b) Box plots showing actual evapotranspiration (mm/season) and biomass (Mt/ha/season) estimates of both models for onion, potato, table grapes, and wheat during the 2021 growing season in the study area within the Litani River Basin in Lebanon.

### 3.1.3. Seasonal Biomass Estimation by WaPOR and GYMEE Models and District-Wise Assessment

Figure 6a shows scatter plots with statistical parameters between biomass derived from GYMEE and FAO WaPOR for onion, potato, table grapes, and wheat in

the 2021 growing season in the study area within the Litani River Basin in Lebanon. A reasonable model agreement is observed for the four crops with high correlation ( $r > 0.9$ ), relatively low RMSE values ( $< 3$  Mt/ha), and low bias ( $MBE < 3$ ). The analysis of  $r$  along with RMSE, and bias shows that GYMEE and WaPOR are at the best agreement when estimating biomass of wheat. Higher divergences were observed between the models when estimating onion and table grapes biomass. The accuracy of estimation of the biomass was not as high for onion (2.7 Mt/ha) and table grapes (2.11 Mt/ha) with RMSEs higher than those of potato (1.66 Mt/ha) and wheat (1.32 Mt/ha). The Relative Error (RE) values show the extent of percentage deviations between modeled estimates, ranging from 9.89% to 24.57% across crops. GYMEE modeled estimates for wheat, table grapes, potato, and onion are on average 9.89%, 12.97%, 14.1%, and 24.57% (RE) higher, respectively, compared to the estimates by WaPOR, indicating a slight potential discrepancy in yield estimation between the models.

Figure 6b shows an inter-comparison of modeled biomass derived from GYMEE and FAO WaPOR for the four analyzed crops onion, potato, table grapes, and wheat in the three producing districts Baalbak, West Bekaa, and Zahleh. The modeled biomass estimates from both GYMEE and WaPOR demonstrate favorable outcomes for all crops when examined at a spatially disaggregated level. These findings align with the biomass analysis presented in Figure 6a with high correlation ( $r > 0.9$ ) and low bias ( $MBE < 3$ ).

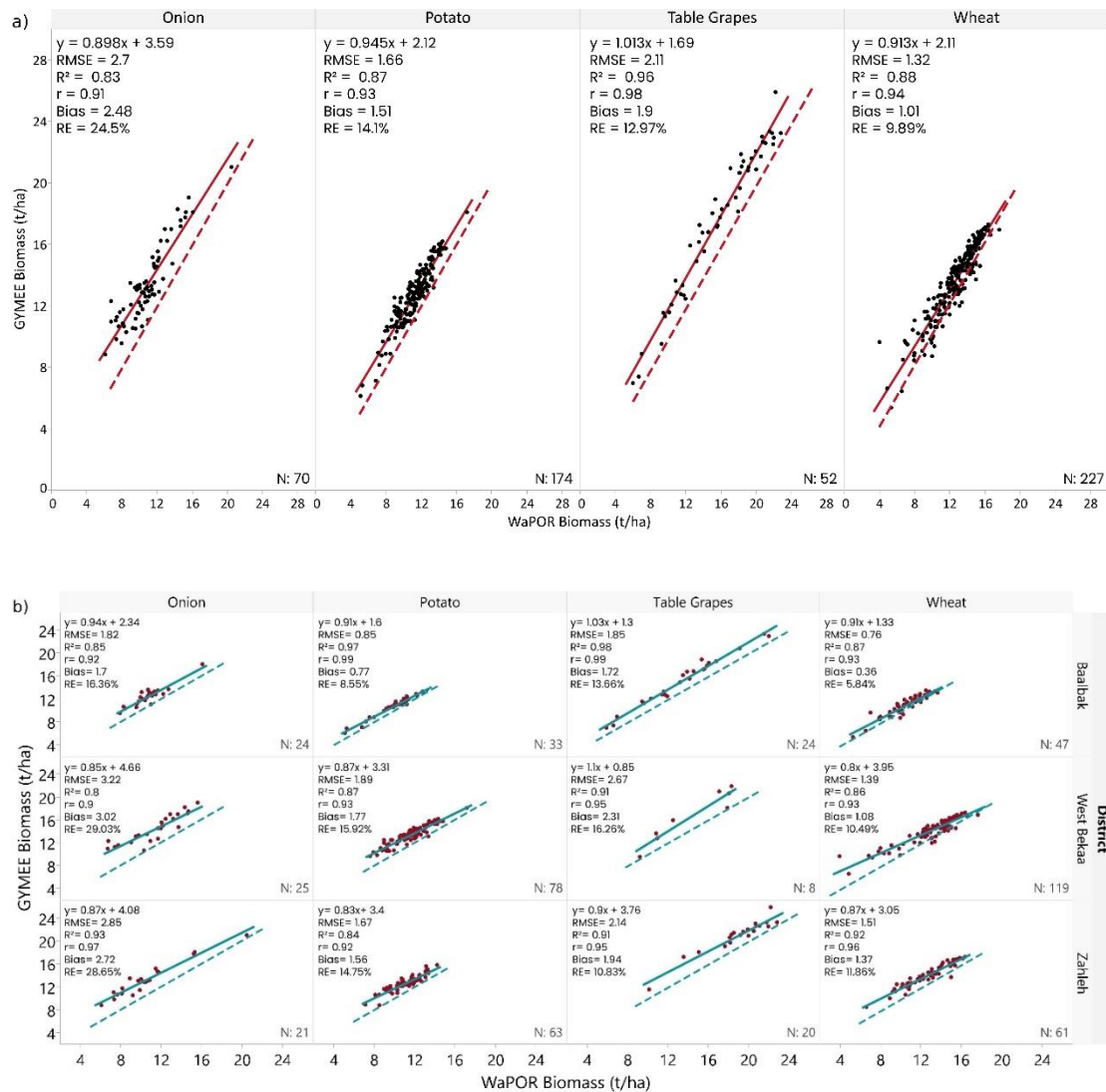


Figure 6. (a) Scatterplots comparing modeled biomass estimates; (b) Scatterplots inter-comparing district-disaggregated modeled biomass derived from GYMEE and FAO WaPOR for onion, potato, table grapes, and wheat in the three producing districts Baalbak, West Bekaa, and Zahleh during 2021 growing season in the study area within the Litani River Basin in Lebanon.

Figure 7 shows bar charts comparing crop yields of onion, potato, table grapes, and wheat using GYMEE and WaPOR models across three producing districts.

GYMEE tends to consistently estimate slightly higher crop yields for all the studied crops in the three districts compared to WaPOR. The basin-scale estimated mean potato yield ranged between 37.9 MT/ha and 50.8 MT/ha, with an average of 42 Mt/ha for the

WaPOR model and 47 Mt/ha for the GYMEE model. The estimated mean wheat yield at the basin level ranged between 2.94 MT/ha and 4.03 Mt/ha, with an average of 3.5 Mt/ha for the WaPOR model and 3.8 Mt/ha for the GYMEE model. These mean estimates demonstrate a moderate reduction in yields compared to the figures (4.58 MT/ha) reported by farmers in the basin back in 2014 (Tawk, Chedid, Chalak, Karam, & Hamadeh, 2019), and closely align with the remote sensing wheat yield estimates (3.2 Mt/ha) reported by Safi et al. (2022). The estimated mean onion yield at the basin level ranged between 61.5 Mt/ha and 84.4 Mt/ha, with an average of 64 Mt/ha for the WaPOR model and 78 Mt/ha for the GYMEE model. The estimated mean table grapes yield at the basin level ranged between 16.7 Mt/ha and 26 Mt/ha, with an average of 20 Mt/ha for the WaPOR model and 22 Mt/ha for the GYMEE model. This result is comparable with the mean table grapes yield (17.86 Mt/ha) reported by Safi et al. (2022).

Among both models, GYMEE exhibits the highest values for onion (84.4 Mt/ha), potato (50.8 Mt/ha), and wheat yields (4.03 Mt/ha) in the West Bekaa district. GYMEE demonstrates the highest yields for table grapes (26 Mt/ha) in Zahleh. Baalbak consistently has lower yields for all crops regardless of the model used.

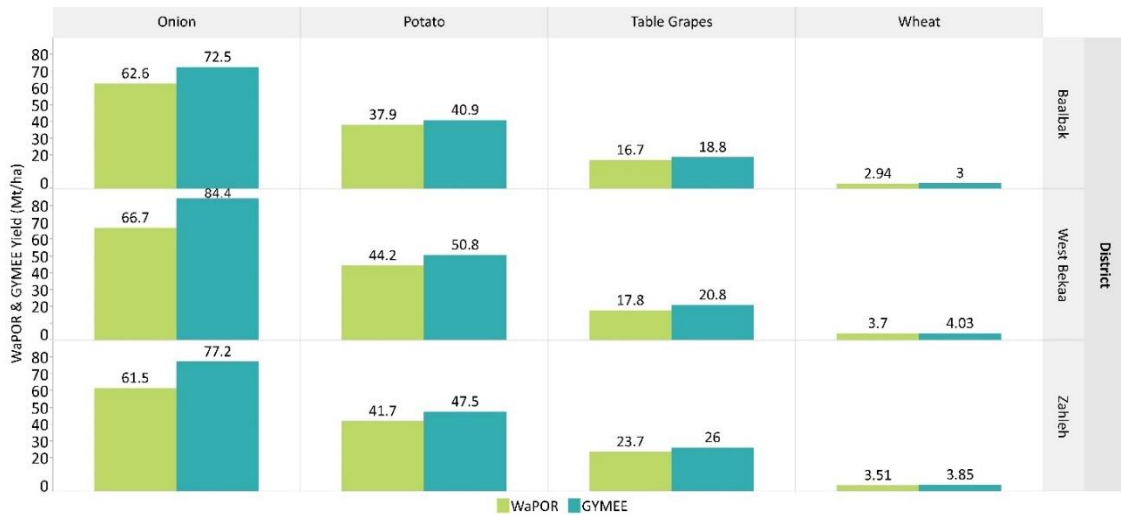


Figure 7. Bar charts comparing crop yields of onion, potato, table grapes, and wheat using GYMEE and WaPOR models across three producing districts Baalbak, West Bekaa, and Zahleh during 2021 growing season in the study area within the Litani River Basin in Lebanon.

### 3.1.4. Seasonal Actual ET Estimation by WaPOR and HSEB Models and District-Wise Assessment

Figure 8a shows scatter plots with statistical parameters between actual evapotranspiration  $ET_a$  derived from HSEB and FAO WaPOR for onion, potato, table grapes, and wheat in the 2021 growing season in the study area within the Litani River Basin in Lebanon. A reasonable model agreement is observed for the four crops in the estimation of  $ET_a$  with moderate to strong correlation ( $0.75 < r < 0.95$ ), relatively low RMSE values ( $< 0.39$  mm/day), and low bias ( $-0.24 < MBE < 0.12$  mm/day). Slightly higher divergences were observed between the models when estimating potato and table grapes biomass. The accuracy of estimation of  $ET_a$  was not as good for potato (59.42 mm/season = 0.39 mm/day) and table grapes (86.56 mm/season = 0.36 mm/day) with RMSEs higher than those of wheat (74.05 mm/season = 0.35 mm/day) and onion (61.72 mm/season = 0.29 mm/day). The Relative Error (RE) values show the slight extent of percentage deviations between seasonal modeled estimates, ranging from 7.29% to 9.28% across crops. The HSEB model yields an average RE of 7.29% higher for onion,

and for wheat, table grapes, and potato, the estimates are comparatively lower by an average of 9.28%, 7.63%, and 7.67%, respectively, when contrasted with the estimations produced by WaPOR.

Similar trends can be noted in Figure 8b, which compares the district-scale ETa values from the HSEB and WaPOR models. The HSEB model tends to produce slightly higher estimates for onion (with a higher RE%), while for wheat, table grapes, and potato, the model's estimates are generally lower across all districts.

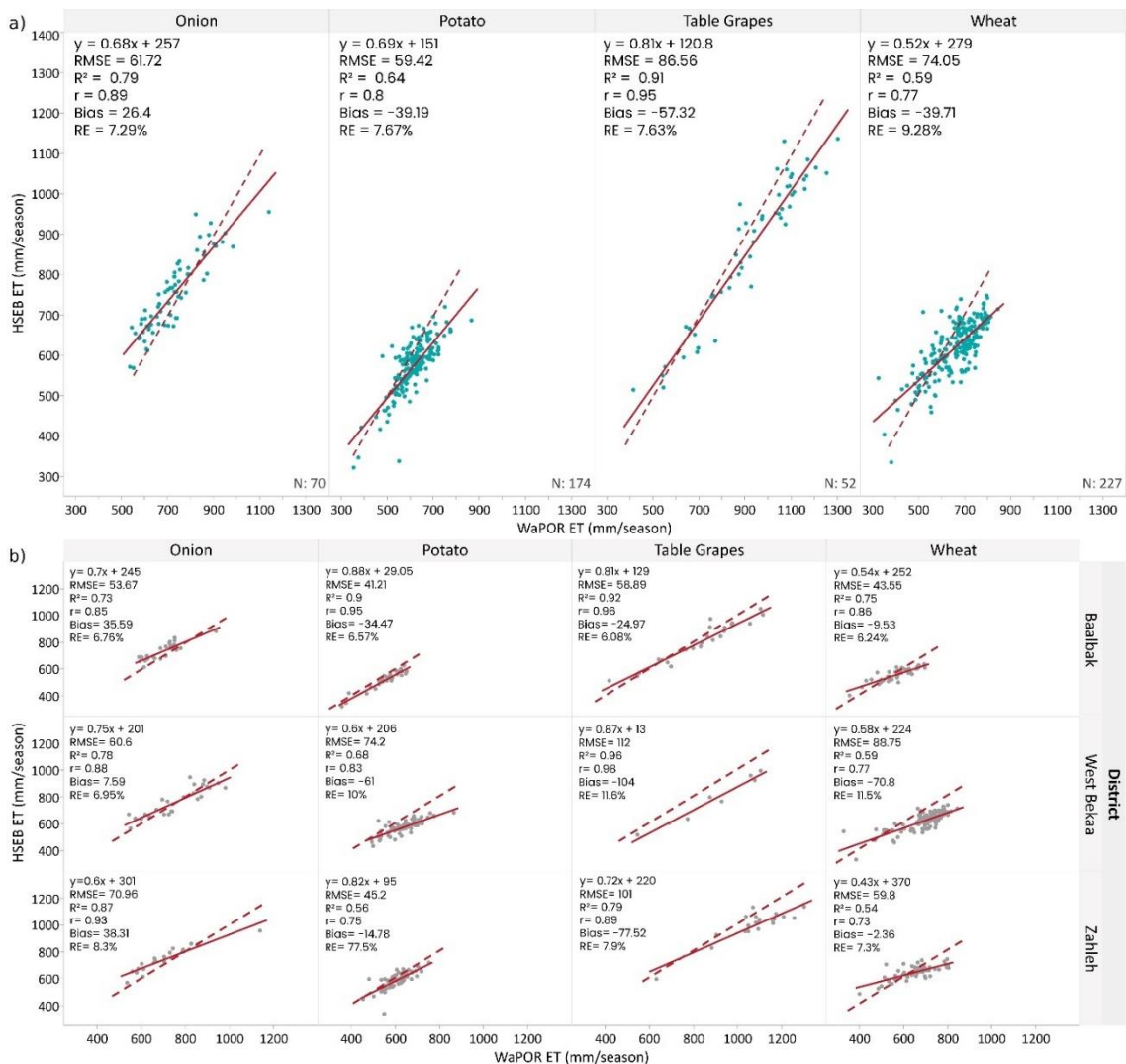


Figure 8. (a) Scatterplots comparing modeled mean actual Evapotranspiration estimates; (b) Scatterplots comparing modeled district-disaggregated actual Evapotranspiration estimates - derived from HSEB and FAO WaPOR for onion, potato, table grapes, and wheat during 2021 growing season in the study area within the Litani River Basin in Lebanon.

Figure 9 shows bar charts comparing actual ET of onion, potato, table grapes, and wheat using HSEB and WaPOR models across three producing districts. WaPOR consistently predicts slightly higher crop ETa values for all the crops under study across the three districts, apart from onion, when compared to HSEB. The basin-scale estimated seasonal mean ETa values for the WaPOR and HSEB models respectively were 725 and 751 mm for onion, 612 and 573 mm for potato, 928 and 871 mm for table grapes, and 660 and 621 mm for wheat.

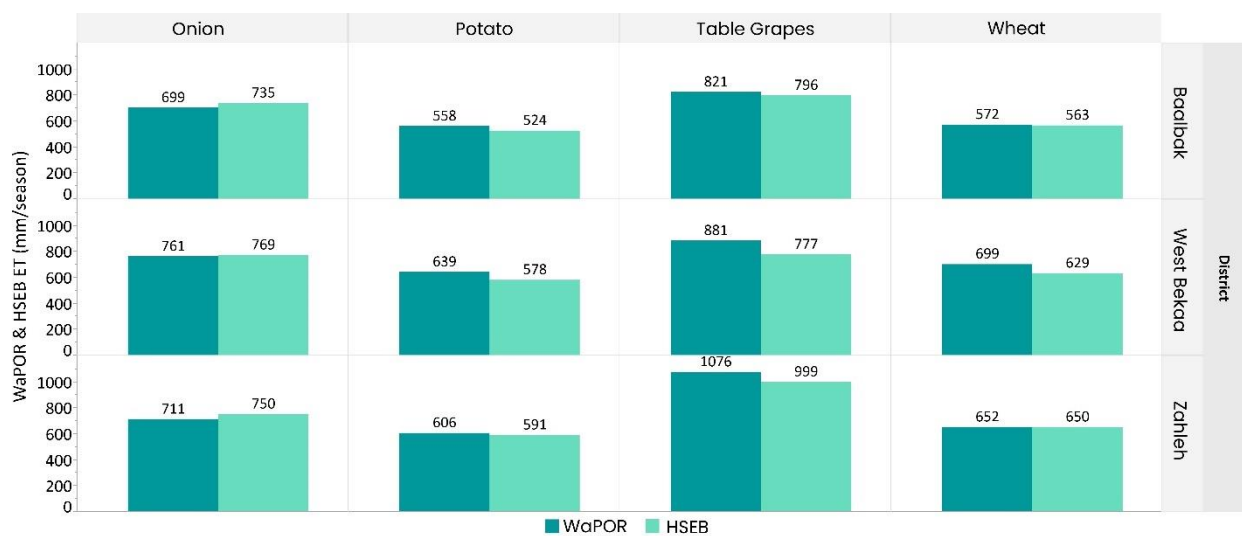


Figure 9. Bar charts comparing actual evapotranspiration of onion, potato, table grapes, and wheat using HSEB and WaPOR models across three producing districts Baalbak, West Bekaa, and Zahleh during 2021 growing season in the study area within the Litani River Basin in Lebanon.

### 3.2. Economic Data Results

Table 4 presents data on the cost of production in the three districts and the net revenues derived from the two remote sensing models – WaPOR and HSEB-GYMEE – of the studied crops. The HSEB-GYMEE model derived-net revenues for all crops are consistently higher compared to the WaPOR model. Net revenues of studied crops vary by district. In Baalbak and West Bekaa, potato tends to have the highest net revenues

across both models, followed by onion, table grapes, and wheat. In Zahleh, potato typically exhibits the highest net returns, followed by table grapes, onion, and wheat.

Inter-comparing model values of one crop type across the three districts, based on both WaPOR and HSEB-GYMEE models, wheat exhibits its highest net returns when cultivated in West Bekaa while exhibiting its lowest in Baalbak. Similarly, potato exhibits its highest net revenues in West Bekaa and its least in Baalbak according to both WaPOR and HSEB-GYMEE models. As for table grapes, the data from both models underscores its peak net revenues when cultivated in Zahleh, whereas its lowest figures are associated with Baalbak. The WaPOR model highlights that onion exhibits its maximum net revenues in West Bekaa, contrasting with its lowest returns found in Zahleh. Meanwhile, under the HSEB-GYMEE model, onion's highest net revenues are tied to West Bekaa, yet its lowest figures are in Baalbak.

In the scenario where farming practices and cultivation factors such as climate, economic conditions, input costs, land rental, technology adoption, and scale of production are relatively spatially similar, a uniform production cost per crop across the three districts is assumed. In terms of variation in production costs across the three districts, potato carries the most substantial cost at \$4,826 per hectare, followed by table grapes at \$4,590 per hectare. Subsequently, onion incurs a cost of \$4,244 per hectare, while wheat records the lowest production cost at \$848 per hectare.

Table 4. District-scale cost of production and net revenues derived from FAO WaPOR and HSEB-GYMEE models for selected crops in the producing districts in 2021.

Crop	District	Production Cost (\$/ha)	WaPOR-Derived Net Revenue (\$/ha)	HSEB-GYMEE-Derived Net Revenue (\$/ha)
<b>Onion</b>	Zahleh	4,244	6,193	8,890
	Baalbak		6,396	8,086
	West Bekaa		7,102	10,097
<b>Potato</b>	Zahleh	4,826	11,813	14,162
	Baalbak		10,382	11,542
	West Bekaa		12,820	15,487
<b>Table Grapes</b>	Zahleh	4,590	10,494	12,034
	Baalbak		6,093	7,457
	West Bekaa		6,814	8,648
<b>Wheat</b>	Zahleh	848	370	449
	Baalbak		178	213
	West Bekaa		502	553

### 3.3. Effect of Model Selection on EIWP Results

Figure 10 shows the variation of mean EIWP values per crop across the three producing districts. Mostly, the mean district HSEB-GYMEE model derived EIWPs are slightly higher than those derived from the WaPOR model. Within districts, EIWP results of wheat generated by both models are very comparable (HSEB-GYMEE EIWPs are equal for Baalbak and are 14% and 11% higher for West Bekaa and Zahleh respectively). The HSEB-GYMEE model produces EIWP values for potato that are approximately 28%, 48%, and 36% higher than those derived from WaPOR in Baalbak, West Bekaa, and Zahleh respectively. When estimating average EIWPs of onion and table grapes, the HSEB-GYMEE model produces EIWP values that are 35% and 33% higher than those derived from WaPOR, respectively.

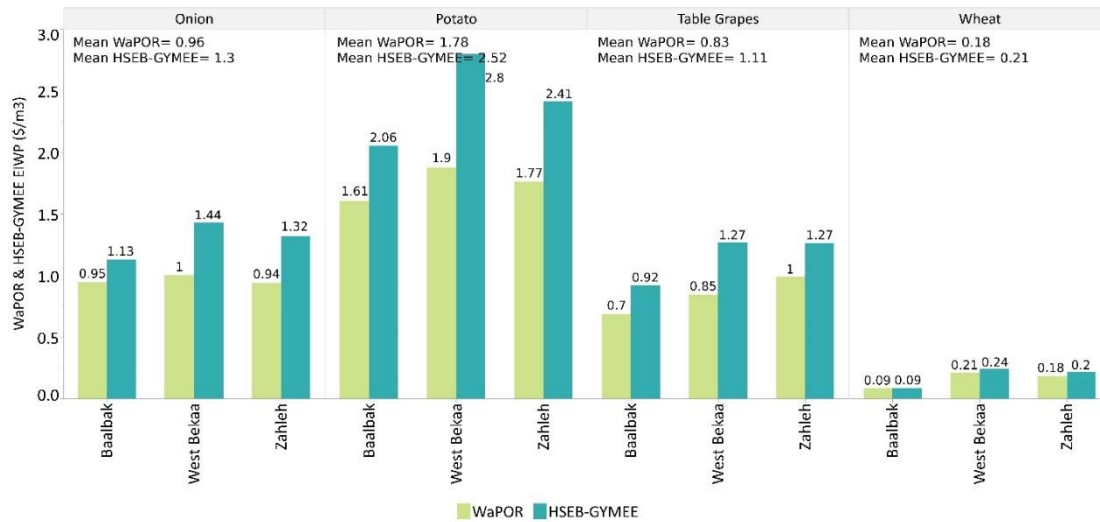


Figure 10. Records of mean EIWP (\$/m<sup>3</sup>) values per crop across the three producing districts in the Litani River Basin in Lebanon.

Within the basin, results reveal that potato is the most economically water-productive crop with highest mean EIWP of 2.52 \$/m<sup>3</sup> and 1.78 \$/m<sup>3</sup> (HSEB-GYMEE and WaPOR respectively). Conversely, wheat is the least economically water-productive crop with mean EIWP of 0.21 \$/m<sup>3</sup> and 0.18 \$/m<sup>3</sup> (HSEB-GYMEE and WaPOR respectively). This indicates a relatively lower economic return for producers from using 1 cubic meter of irrigation water on wheat. Onion and table grapes hold the second and third positions among economically water-productive crops in the basin, respectively. The ranking of crop EIWP remains consistent across the districts of Baalbak, West Bekaa, and Zahleh.

# CHAPTER 4

## DISCUSSION

### 4.1. Economic Irrigation Water Productivity Analysis

In this study, we explore the economic irrigation water productivity (EIWP) of four crops within the Litani River Basin in Lebanon, comparing the results obtained from different remote sensing models and examining the influence of these models on EIWP outcomes. First, our findings reveal that mean EIWP values of all four crops are positive, implying that the benefits of production exceed the costs of production associated with the water used for irrigation. Second, when comparing the model-derived EIWP values of HSEB-GYMEE (WaPOR), interesting patterns emerge - results reveal that the EIWP of potato is respectively 12 (10) times higher than the EIWP of wheat, 2.2 (2.1) times higher than the EIWP of table grapes respectively, and 1.9 (1.85) times higher than the EIWP of onion respectively. The difference in EIWP is a good indicator to improve the economic value of irrigation water. Achieving this could involve strategic interventions to reduce evaporative losses in actual evapotranspiration or implementing practices that optimize crop cultivation while managing controlled water stress through efficient irrigation scheduling.

Third, although onion produces on average more marketable biomass (yield) than potato (figure 7) and consumes more irrigation water (figure 9), the former's average EIWP remains lower. There is potential to improve water management by diverting water away from agricultural areas with the lowest EIWP, as having a higher EIWP implies that the crops have used less water footprint. Additionally, there is potential to replace the cultivated variety with other less water-consuming varieties of

onion. Despite having the highest production costs, potato demonstrates the highest EIWP results within the basin. However, the sensitivity of EIWP to market prices and the importance of diversifying crops for farmer's risk management suggest that cultivating the most productive crop alone may not be a desirable strategy, as basin-wide monoculture practices are not favored by farmers who aim to spread the risks associated with price variations and disease outbreaks.

Fourth, increases in economic water productivity may indicate a shift towards higher valued crops, increase in yields or a saving in water input (Bos, Burton, & Molden, 2005). Although our results show that wheat has the advantage of having the lowest production cost compared to other crops in the basin, which could make it an attractive choice for farmers due to its low initial investment, it also has the lowest EIWP in all districts according to both the HSEB-GYMEE and WaPOR models. This low EIWP implies that wheat does not generate significant economic value in terms of crop output for the irrigation water it requires, hence the potential revenue generated from the crop does not justify the water resources invested. This makes wheat a less financially promising choice for cultivation, as farmers in the basin are currently shifting to other grains such as barley cultivation, despite wheat's lower production costs.

## **4.2. Potential Sources of Modeled Biomass and ET Differences**

### ***4.2.1. Beyond Reference Evapotranspiration***

Our assessment of Reference Evapotranspiration (ET<sub>ref</sub>) values from both HSEB and WaPOR ET models reveals that, on average, the WaPOR model demonstrates a difference that is 17% higher than that of the HSEB model (Section 3.1).

ET<sub>ref</sub> represents evapotranspiration from a hypothetical reference crop, imitating the characteristics of a well-watered grass surface. This approach allows estimation of potential ET for various crops through the application of predefined crop coefficients. Our results suggest that the bias in model outputs stems from differences in the subsequent conversion from ET<sub>ref</sub> to ET<sub>a</sub>, rather than being primarily attributed to the slight differences in ET<sub>ref</sub> values derived by each model. Both models determine ET<sub>ref</sub> using the Penman-Monteith equation, however WaPOR utilizes weather data sourced from the daily 19 Km spatial resolution MERRA dataset up to the start of GEOS-5 (2014) for the derivation of ET<sub>ref</sub> (FAO, 2020), while HSEB utilizes the ECMWF ERA5-Land hourly 9 Km spatial resolution dataset. This could result in variations in factors such as temperature, humidity, wind speed, and solar radiation, which are components of the Penman-Monteith equation used to calculate ET<sub>ref</sub>. The FAO WaPOR employs a global atmospheric model to provide meteorological information. However, this approach has limitations, which encompass uncertainties tied to the spatial variability and resolution of this data. For instance, temperature data are available at a spatial resolution of 0.25 degrees (approximately 28 Km at the equator), while HSEB utilizes 0.1 degrees hourly ECMWF with 9 Km resolution and downscales it to 90 m.

#### ***4.2.2. Environmental Stressors of the Models' Biomass and ET Equations***

The choice of remote sensing model for agricultural water management can impact decision making in several ways. Our comparative results reveal consistently slightly higher biomass values produced by the GYMEE model (Section 3.1), despite its lower LUE<sub>max</sub> (2.5 g/MJ) than WaPOR's (2.7 g/MJ) and despite having a common

fPAR equation across WaPOR and GYMEE (Section 2.2.2.i.). The difference in LUEmax values between the WaPOR and GYMEE models may have implications for their respective biomass estimations. A higher LUEmax value in the WaPOR V2 model (2.7) implies that under optimal conditions, WaPOR assumes a more efficient photosynthetic conversion process compared to GYMEE's LUEmax (2.5). This means that WaPOR attributes a greater biomass production potential for the same amount of absorbed light energy. Knowing that, the results suggest that other factors within the models, such as stress effects, are playing a significant role in driving these differences. The likely factors contributing to the higher biomass values from the GYMEE model would involve the combined effects of the stress factors, vapor stress and temperature stress, the unit conversion factor (0.864), and any other model-specific parameterizations. Local factors, such as specific environmental conditions and crop management practices, could also influence the model performance. The GYMEE biomass model, by considering vapor and temperature stress, could potentially provide estimates responsive to varying environmental conditions. However, this complexity in stress estimation could make the biomass model harder to implement. The WaPOR biomass model's equation on the other hand is simpler due to the absence of stress factors, making it easier to apply but potentially less adept at encompassing environmental effects. In regions with stable environmental conditions, where stress factors play a minor role, both models might provide similar results. In regions with significant environmental variations, the GYMEE model, which has a global extent, might be more suitable due to its ability to account for stress effects. The presence of vapor and temperature stress factors in the GYMEE equation might lead to a more

nuanced response to changing environmental conditions. The absence of these factors in the WaPOR equation could result in less variability in calculated biomass values.

As for variations in actual ET outputs, our results show that WaPOR V2 was producing slightly higher ET<sub>a</sub> estimates than HSEB for most crops, wheat (9.28%), table grapes (7.63%), and potato (7.67%), while for onion the HSEB model produces an average RE of 7.29% higher than WaPOR (Section 3.1). This could be attributed to the uncertainty stemming from the reduced number of satellite scenes during the fourth month in the HSEB model, which is restricted to two scenes due to cloud cover. The methodology for computing aerodynamic resistance to heat transfer for determining relative soil moisture (Se) within the soil moisture stress component of the WaPOR V2 model is based on equations A1 (full canopy), A6 (bare), and A7 (soil) from Sánchez, Kustas, Caselles, and Anderson (2008). The calculation of T<sub>cmax</sub>, representing the surface temperature for the driest fully vegetated surface, involves the aerodynamic resistance, which is influenced by wind speed derived from GEOS-5 and ERA5 model data. However, under specific circumstances, GEOS-5 and ERA5 wind speeds can unrealistically decrease. Increases in surface heat flux result in turbulence, creating negative feedback on heat flux and surface temperature. This turbulent heat flux feedback mitigates elevated heat flux and surface temperature. The WaPOR V2 model hence lacks this turbulent heat flux. Consequently, situations with very low wind speeds (below 1 m/s) coexisting with elevated heat flux, lead to unrealistically high surface temperatures. This feedback could potentially contribute to ET<sub>a</sub> values surpassing those from HSEB. While these factors could explain the variation in outputs found with FAO WaPOR and HSEB-GYMEE in 2021, further research is required for a better understanding of such discrepancies across different years.

## CHAPTER 5

### CONCLUSION

This paper underscores the significance of biomass and ET model selection in determining EIWP for various crops on a basin-wide scale. We examine and compare the actual evapotranspiration (ET<sub>a</sub>), biomass, yield, economic variables, and Economic Irrigation Water Productivity (EIWP) for four crops - potato, wheat, onion, and table grapes - in three districts within the Litani River Basin (West Bekaa, Zahleh, and Baalbak) in 2021 as derived from HSEB-GYMEE and WaPOR models. The mean monthly ET<sub>a</sub> and biomass estimations for all crops, derived from both models, exhibit a high degree of similarity. The comparative analysis of crop ET<sub>a</sub> values across three districts reveals that WaPOR consistently produces slightly higher ET<sub>a</sub> values for most studied crops, when compared to HSEB. Contrary to the ET<sub>a</sub> results, the GYMEE model consistently estimates slightly higher mean biomass values for all studied crops compared to WaPOR in the three districts. The economic irrigation water productivity (EIWP) values produced by both models consistently indicate that potato holds the highest EIWP across all districts, followed by onion, table grapes, and wheat. The dissimilarities found between the models arise from differences in the consideration of environmental stressors (vapor stress and temperature stress), conversion factors, and in the calculation method for soil moisture stress. Thus, when comparing magnitudes and trends of biomass and ET<sub>a</sub> between the different approaches it is not within the scope of this research to assess the accuracy of one model relative to others, specifically since there is limited ground observations to validate the data.

Using economic water productivity indicators enhances on-farm irrigation decision-making (Fernández, Alcon, Diaz-Espejo, Hernandez-Santana, & Cuevas, 2020). Poor policies and lacking coordination across scales impede systemic shifts in agricultural water use, exacerbating water scarcity (Uhlenbrook, Yu, Schmitter, & Smith, 2022). Basin and national efforts to reduce crop water consumption through regulation can yield paradoxical outcomes. Evidence-backed agricultural water policies focusing on EIWP may induce farmer behavior changes, curbing water use increases. Although increasing EIWP is not necessarily in agreement with the objectives of individual farmers as to net revenue or the amount of output generated, it remains useful in basins where water is scarce and irrigation management is crucial. The study provides a foundation for future research on the impact of remote sensing models in other water-stressed and socioeconomically challenged basins. The implications of our comparative study can be translated into strategies based on model selection. These strategies can help farmers contribute to a more sustainable water resource management for increased production and future seasons, thereby enhancing both yield and income prospects. Achieving this goal necessitates a comprehensive examination of policy implications, a transparent acknowledgment of limitations, and the provision of practical recommendations.

## APPENDIX 1

Table 1A. Comparative analysis of GYMEE and WaPOR biomass equations through dissection of data components and environmental stressors.

<b>Data Component</b>	<b>GYMEE Biomass methodology detailed in Jaafar &amp; Mourad (2021)</b>	<b>WaPOR Biomass methodology based on the C-Fix Model Detailed in <a href="#">Veroustraete et al. (2002)</a></b>
Yield Equation (kg/ha)	$Y = \frac{AGBs \times HI \times C_4}{(1 - m_c)}$ <p>Where:  <b>AGBs</b>: Seasonal Above ground biomass  <b>HI</b>: Harvest Index  <b>Mc</b>: Moisture content</p>	$Y = \frac{AGBs \times HI \times C_4}{(1 - m_c)}$ <p>Where:  <b>AGBs</b>: Seasonal Above ground biomass  <b>HI</b>: Harvest Index  <b>Mc</b>: Moisture content</p>
Seasonal Above Ground Biomass AGBs needed for yield	$AGB_s = \sum_{i=SOs}^{EOS} DMP_i \times Nd(i)$	$AGB_s = \sum_{i=SOs}^{EOS} DMP_{(i)} \times Nd(i)$ <p>WaPOR Total Biomass Production (TBP), here labeled as AGBs, is defined as the sum of the above-ground dry matter produced during the crop growing season. Nd: number of days within each dekad, varying between 8 (end of February) and 11</p>
Above-Ground Dry Matter Production (DMP) (kg/ha)	$DMP = APAR \times LUE_{max} \times SM \times VS \times TS \times 0.864$ <p>Where:  DMP is labeled as AGB in GYMEE Jaafar &amp; Mourad (2021)  APAR: absorbed photon flux by the canopy photosynthetic elements  LUE: Light Use Efficiency  0.864: unit conversion factor <a href="#">Silva et al. (2018)</a></p>	$DMP = NPP \times 22.222$ $DMP = APAR \times LUE_{max} \times SM \times 0.63$ <p>Where:  DMP (Kg/ha)  <b>NPP</b>: Net Primary Production  1 gC/m<sup>2</sup>/day (NPP) = 22.222  kgDM/ha/day (DMP) (Ajtay et al., 1979)</p>

<p>Light Use Efficiency (<b>LUE</b>)</p>	$LUE = LUE_{max} \times TS \times VS \times SM$ <p>Where:  <b>LUE<sub>max</sub></b>: maximum Light Use Efficiency (g/MJ)  <b>TS</b>: Temperature Stress  <b>VS</b>: Vapor Stress  <b>SM</b>: Soil Moisture Stress</p>	<p>Since soil moisture stress is already added to the NPP calculation of WaPOR, the <b>LUE used in WaPOR is the LUE<sub>max</sub></b>  <math>LUE = LUE_{max}</math></p> <p>Light use efficiency is used as an input to convert the maximum NPP value to actual NPP.  <a href="#">pyBiomass (2022)</a></p> <p>Land Cover specific Light Use Efficiency (LUE) values based on WaPOR L3 Land Cover Classification; If L3 LC was not yet available, preliminary LC obtained from ESA WorldCover Land Cover product is used; LUE is static and is not computed as intermediary, rather is involved directly in the computation of NPP. <a href="#">Copernicus (2022)</a></p>
<p><b>LUE<sub>max</sub></b></p>	<p><b>LUE<sub>max</sub> = 2.5 g/MJ</b>  For C3 crops potato and wheat</p>	<p><b>LUE<sub>max</sub> = 2.7 g/MJ</b>  For croplands <a href="#">pyBiomass (2022)</a> and <a href="#">WaPOR Biomass Data Manual V2.0.</a></p>
<p>Net Primary Production (<b>NPP</b>) (gC/m<sup>2</sup>)</p>	$NPP = APAR \times LUE_{max} \times TS \times VS \times SM$	<p>At the end of every dekad, a new data layer: NPP<sub>max,10</sub> is computed with the mean of the daily NPP<sub>max,1</sub> scenes. Next, NPP<sub>max,10</sub>, fAPAR, the land use efficiency and SM are simply multiplied to retrieve the final dekadal NPP output. <a href="#">pyBiomass (2022)</a></p> <p>NPP is delivered on a dekadal basis, where pixel values represent the average daily net primary production for that specific dekad in gC/m<sup>2</sup>/day. The method to compute Net Primary Production is based on Monteith (1972).</p> $ \begin{aligned} NPP &= fPAR \times SM \times \epsilon LUE \\ &\quad \times NPP_{max} = S_c \times R_s \\ &\quad \times \epsilon_p \times fPAR \times SM \\ &\quad \times \epsilon LUE \times \epsilon T \times \epsilon CO_2 \\ &\quad \times \epsilon AR \times \epsilon RES \\ &= fPAR \times SM \times 2.7 \\ &\quad \times 0.45 \times PAR_{daily} \times 1 \\ &\quad \times 1.26 \times 0.5 \times \epsilon T = \\ NPP &= APAR \times LUE_{max} \times SM \times \\ &\quad \mathbf{0.63} \times S_c \end{aligned} $

		<p>Where:</p> $NPP_{max} = S_c \times R_s \times \epsilon_p \times \epsilon_T \times \epsilon_{CO2} \times \epsilon_{AR}$ $= S_c \times PAR_{daily} \times 1 \times 1.26 \times 0.5$ <p>Where:</p> <p><b>S<sub>c</sub></b>: conversion factor from DM to C [gC/gDM] 1 gC/m<sup>2</sup>/day (NPP) = 22.222 kgDM/ha/day (DMP).</p> <p><b>R<sub>s</sub></b>: Total shortwave incoming radiation in the form of solar energy (GJT/ha/day); provided on a daily basis</p> <p><b>ε<sub>p</sub></b>: Climatic Efficiency; constant= 0.48 (JP/JT) (denoting that 48% of all incoming solar radiation is situated in the 400-700nm region)</p> <p><b>fPAR</b>: Fraction of Absorbed Photosynthetically Active Radiation (JPA/JP)</p> <p><b>SM</b>: Soil moisture stress reduction factor</p> <p><b>εLUE</b>: Light use efficiency at optimum conditions (Kg DM/GJPA); is a coefficient for the efficiency by which vegetation converts energy into biomass = 2.7</p> <p><b>εT</b>: 1: Normalized temperature effect (provided on a daily basis; GEOS-5 Data Product <a href="#">PyBiomass2022</a>)</p> <p><b>εCO2</b>: 1.26: Normalized CO2 fertilization effect; usually assumed to be constant over the globe, as well as within a year.</p> <p><b>εAR</b>: Fraction kept after autotrophic respiration= 0.5</p> <p><b>εRES</b>: fraction kept after residual effects = 1 (constant)</p> <p><b>NPP<sub>max</sub></b>: maximum obtainable NPP calculated on a daily basis, for the (virtual) cases where fAPAR would be equal to one.</p>
<p><b>εAR</b> Fraction kept after autotrophic respiration</p>	<p>N/A</p>	$\epsilon_{AR} = \frac{7.825 - 1.145 T_a}{100}$ <p>Based on <a href="#">Veroustraete et al. (2002)</a></p> <p>εAR depends only on temperature in WaPOR V2.0 based on <a href="#">Veroustraete et al.</a></p>

		<p>(2002) C-Fix Model. While in V3.0, it is updated to include other parameters: 1) slope to determine autotrophic respiratory fraction; 2) intercept to determine autotrophic respiratory fraction; 3) daily air temperature.</p> <p>Taken as constant = 0.5 in WaPOR model <a href="#">PyBiomass2022</a></p> <p>Where:  <b><math>\epsilon_{AR}</math></b>: fraction of assimilated photosynthates consumed by autotrophic respiration.  <b>Ta</b>: Atmospheric Temperature</p>
<p><b><math>\epsilon_{CO2}</math></b>  <b>Normalized CO2 fertilization effect</b></p>	N/A	<p><math>CO_{2fert} = [CO_2] - [O_2]2\tau[CO_2]^{ref} - [O_2]2\tau K_m 1 + [O_2]K_0 + [CO_2]^{ref} K_m 1 + [O_2]K_0 + [CO_2]^{ref} K_0</math></p> <p>CO2 fertilization effect is temperature dependent. For C-Fix Model, the below parameter values are used at 25 °C. Based on <a href="#">Veroustraete et al. (2002)</a></p> <p>Where:  <b><math>\epsilon_{CO2}</math></b>: 1.26: Normalized CO2 fertilization effect  <b><math>\tau</math></b>: 2550: CO<sub>2</sub>/O<sub>2</sub> specificity ratio  <b>K<sub>m</sub></b>: 948: Affinity constant for CO<sub>2</sub> of Rubisco  <b>K<sub>0</sub></b>: 30: Inhibition constant for O<sub>2</sub>  <b>[O<sub>2</sub>]</b>: 20.9  <b>[CO<sub>2</sub>]</b>: CO<sub>2</sub> concentration in the mesophyll tissue of leaves  <b>[CO<sub>2</sub>]<sup>ref</sup></b>: 281</p>
<p><b><math>\epsilon_T</math></b>  <b>Normalized temperature effect</b></p>	N/A	$\epsilon_T = \frac{e^{(C1 - \frac{\Delta H_{a,P}}{R_g T})}}{1 + e^{\frac{(\Delta S T - \Delta H_{d,P})}{R_g T}}}$ <p>Based on <a href="#">Veroustraete et al. (2002)</a></p> <p>Values of <b><math>\epsilon_T</math></b> range from 0 to 1. In C-fix at 25°C, <b><math>\epsilon_T</math></b> is around 1.</p> <p>Where:  <b><math>\epsilon_T</math></b>: normalized temperature effect [-]  <b>C1</b>: 21.77 (constant)  <b><math>\Delta H_{a,P}</math></b>: 52,750: Activation energy in (J/ mol)  <b>R<sub>g</sub></b>: 8.31: Gas constant in J/ (K. mol)  <b>T<sub>opt</sub></b>: 295.13: Air temperature (K)  <b><math>\Delta S</math></b>: 704.98: Entropy of the denaturation equilibrium of CO<sub>2</sub> in (J/k.mol)  <b><math>\Delta H_{d,P}</math></b>: 211,000: Deactivation energy in</p>

		(J / mol)
<b>APAR</b>	$APAR = fPAR \times PAR_{daily}$ <p>Where:  <b>APAR</b>: Fraction of Absorbed Photosynthetically Active Radiation  <b>fPAR</b>: Fraction of Photosynthetically Active Radiation  <b>PAR<sub>daily</sub></b>: Daily Photosynthetically Active Radiation</p>	$APAR = fPAR \times PAR_{daily}$ <p>Where:  <b>APAR</b>: Fraction of Absorbed Photosynthetically Active Radiation  <b>fPAR</b>: Fraction of Photosynthetically Active Radiation  <b>PAR<sub>daily</sub></b>: Daily Photosynthetically Active Radiation</p>
<b>fPAR</b>	$fPAR = 1.257NDVI - 0.161$	$fPAR = 0.8642NDVI - 0.0814$ <p>Based on <a href="#">Veroustraete et al. (2002)</a></p> <p>Which is being updated to <math>fPAR = 1.257NDVI - 0.161</math> in WaPOR V3.0 similar to that used in <a href="#">GYMEE pyBiomass (2022)</a></p>
<b>PAR<sub>daily</sub></b>	$PAR_{daily} = 0.48 \times Ra \times \tau w$ $= K_{solar} \times 0.48$ <p>Where:  <b>K<sub>solar</sub></b>: solar time-period</p> <p>and  <math display="block">K_{solar} = \tau w \times R_a</math> and  <math display="block">\tau w = R_a \times R_s</math> <p>Where:  <b>R<sub>s</sub></b>: Shortwave Radiation  <b>R<sub>a</sub></b>: daily extraterrestrial solar radiation  <b>τw</b>: Transmissivity</p> </p>	$PAR_{daily} = K_{solar} \times 0.48$ <p>and  <math display="block">K_{solar} = Transmissivity_{24} \times R_{A\_mountain\_24}</math> <p>and  <math display="block">Transmissivity_{24} = R_{A\_mountain\_24} \times R_s</math> <p>Where:  <b>PAR</b>: Photosynthetically Active Radiation; the solar radiation in the spectral range from 400-700 nm that is used by plants for photosynthesis (W/m2).  <b>0.48: ε<sub>p</sub></b>(constant) (ratio par/solar radiation)  <b>K<sub>solar</sub></b>: daily solar radiation (W/m2)</p> </p></p>

		<p><b>Rs:</b> Incoming shortwave radiation product of Meteosat Second Generation (MSG) used to calculate daily transmissivity</p> <p><b><math>R_{A\ mountain\_24}</math>:</b> daily solar radiation at top of atmosphere for a flat surface (W/m<sup>2</sup>)</p> <p><a href="#">PyWaPOR</a> and <a href="#">pyBiomass 2022</a></p>
NDVI data sources	Landsat, Sentinel	<p>1)NDVI at Level 3 is based on both Sentinel-2 and Landsat bottom of atmosphere reflectance data; 2) atmospheric correction is done using SMAC; 3) clipping to the extent of the Level 3 ROI plus a buffer area with cloud masking; 4) data gap filling by interpolating the values of the pixels using the Neighborhood Similar Pixel Interpolator by <a href="#">Weiss, Daniel J., et al. (2014)</a> following <a href="#">Chen et al. (2011)</a>; 5) NDVI ratio is calculated and dekadal NDVI composites are created using the spatio-temporal fusion model which uses the level 1 data (with higher temporal availability) to predict level 3 pixel values at a higher temporal resolution <a href="#">Hazaymeh and Hassan (2015)</a></p> <p>NDVI Data Source: L1TP Data Product from Sensors: Landsat 5 TM; Landsat 7 ETM+; Landsat 8 OLI; Daily</p>
<b>Soil Moisture (SM)</b>	$SM = \frac{T_{act24}}{T_{pot24}}$ <p>Where:  <b><math>T_{act24}</math>:</b> Actual daily transpiration  <b><math>T_{pot24}</math>:</b> Potential daily transpiration</p>	$SM = Ksf \times Se - \left( \frac{\sin(2\pi \times Se)}{2\pi} \right)$ <p>as defined in American Society of Civil Eng (ASCE, 1996), and is derived on a daily basis. The purpose is to compute the reduction in biomass production due to limited water availability. It is based on the trapezoid method by <a href="#">Yang et al. (2015)</a> which improved the Triangle method by <a href="#">Carlson (2007)</a>.  <a href="#">PyBiomass 2022</a></p> <p>Where:  <b>Ksf:</b> Tenacity factor for drought-sensitive plants. A default value of 1.5 in WaPOR V2. For V3.0., a value of 1.0 is being tested.  <b>Se:</b> relative soil moisture content of a specific location</p>

<p><math>T_{pot24} = (1 - e^{(\epsilon \times LAI)}) \times ETP24</math></p> <p>Where:  <math>\epsilon</math>: Light Use Extinction Factor  <math>LAI = \frac{\ln(-f_c - 1)}{-0.45}</math>  <math>f_c = 1 - \left(\frac{0.8 - NDVI}{0.8 - 0.125}\right)^{0.7}</math></p> <p><b>ETP24</b>: is set equal to ET24 if the latter is higher than ET<sub>ref</sub> or to ET<sub>ref</sub> otherwise. A DEM is used to calculate the slope, the aspect of terrain, and solar angles (latitude, declination, solar zenith angle, and solar incidence angle), to adjust land surface temperature (LST) and to correct ET<sub>ref</sub> in the sloped terrains.</p>	<p><math>Se = \frac{(1 - Fc) \times (Ts_{max} - Tc_{max}) + Tc_{max} - LST}{(LST - Tmin) + ((1 - Fc) \times (Ts_{max} - Tc_{max}) + Tc_{max} - LST)}</math></p> <p><b>Se</b>: Relative soil moisture for a specific location  <b>Fc</b>: full vegetation coverage with range from 0 to 1  <b>Tsmax</b>: surface temperatures for the driest bare soil surface  <b>Tcmax</b>: surface temperatures for the driest fully vegetated surface  <b>Tmin</b>: surface temperature for the cold edge, provided on a daily basis  <b>LST Data Source</b>: L1TP Data Product from Sensors: Landsat 5 TM; Landsat 7 ETM+; Landsat 8 OLI</p> <p><math>Fc = 1 - \left(\frac{NDVI_{max} - NDVI}{NDVI_{max} - NDVI_{min}}\right)^n</math>  <a href="#">Yang et al. (2013)</a>  Where:  <b>NDVI<sub>max</sub></b>: NDVI for fully vegetated surfaces = 0.89  <b>NDVI<sub>min</sub></b>: NDVI for bare soil = 0.1  <b>n</b>: is a function of leaf orientation distribution within the canopy, the value of which typically ranges from 0.6 to 1.25</p>
<p><math>T_{act24} = \left(\frac{T'_{act24}}{T'_{act24} + E_{act24}}\right) \times ET_{24}</math></p> <p>Where:  <b>T'act24</b>: first estimate of actual daily transpiration  <math>T'_{act24} = \Psi_{\theta} \times T_{pot24}</math>  <math>\Psi_{\theta} = \frac{\theta_{Vnormalized\ trigger} \sin(2\pi \times \theta_{Vnormalized\ trigger})}{2\pi}</math>  <math>\theta_{Vnormalized\ trigger} = \frac{\theta_{RZ1} - \theta_{PWP}}{\theta_{Vstress\ trigger} + 0.02 - \theta_{PWP}}</math></p>	<p><b>Tcmax</b>: surface temperatures for the driest fully vegetated surface</p> <p><math>T_{c,max} = \frac{(1 - \alpha_c)S_d + \epsilon_c \epsilon_a \sigma T_a^4 - \epsilon_c \sigma T_a^4}{4\epsilon_c \sigma T_a^3 + \rho C_p / r_{a,c}} + T_a</math></p> <p>Where:  <b><math>\alpha_c</math></b>: albedo for fully vegetated surfaces (canopy) = 0.24 <a href="#">Yang et al. (2013)</a>  <b>S<sub>d</sub></b>: downward shortwave radiation (W m<sup>-2</sup>) <a href="#">Allan et al. (1998)</a>  <b><math>\epsilon_c</math></b>: vegetation emissivity (0.985) <a href="#">Yang et al. (2013)</a>  <b><math>\epsilon_a</math></b>: atmospheric emissivity <a href="#">Brutsaert (1975)</a>  <b><math>\sigma</math></b>: Stefan-Boltzmann constant (5.67×10<sup>-8</sup> W m<sup>-2</sup> K<sup>-4</sup>)  <b>T<sub>a</sub></b>: air temperature</p>

<p><b><math>\theta_{Vstress\ trigger}</math></b>  <math display="block">= \theta_{FC}</math> <math display="block">- p\ factor \times (\theta_{FC}</math> <math display="block">- \theta_{PWP})</math></p> <p><b><math>\theta_{PWP}</math></b> : Soil moisture at Permanent Wilting Point  <b><math>\theta_{FC}</math></b>: Soil moisture at Field Capacity  <b><math>p\ factor</math></b> = <math>DF + 0.04 \times (5 - ET_{24})</math>  <b>DF</b>: Crop-dependent depletion factor (0.3 for shallow-rooted plants to 0.7 for deep-rooted plants).</p> <p><b><math>\theta_{RZ1}</math></b>  <math display="block">= \frac{\theta_V - (\theta_{SMtopmean} + \theta_{SMtopstd}) \times (1 - fc)}{fc}</math></p> <p><b><math>\theta_{RZ1}</math></b>: First Estimate of the Root Zone Soil Moisture  <b>Fc</b>: Fraction of vegetation cover  <b><math>\theta_V</math></b>: total soil moisture  <math display="block">\theta_V = \theta_{SMsub} \times e^{\left(\frac{EF_t - a}{b}\right)}</math> <b><math>\theta_{SMsub}</math></b>: saturated soil moisture level  <b>a and b</b>: curve fitting parameters = 1 and 0.421  <math display="block">Max_{\theta_{VRZ}} = fc \times (\theta_{VRZmax} - \theta_{VRZmean}) + \theta_{VRZmean}</math> <b>EF</b>: instantaneous evaporation fraction</p>	<p><b><math>\rho</math></b>: air density (<math>kg\ m^{-3}</math>)  <b><math>C_p</math></b>: specific heat of air at constant pressure (<math>J\ kg^{-1}\ K^{-1}</math>)  <b><math>r_{a,c}</math></b>: aerodynamic resistance to heat transfer between canopy and the reference height (<math>m\ s^{-1}</math>)</p> <p><b>Tsmax</b>: surface temperatures for the driest bare soil surface  <math display="block">T_{s,max} = \frac{(1 - \alpha_s)S_d + \epsilon_s \epsilon_a \sigma T_a^4 - \epsilon_s \sigma T_a^4}{4\epsilon_s \sigma T_a^3 + \rho C_p / [(r_{a,a} + r_{a,s})(1 - G/R_{n,s})]} + T_a</math></p> <p><b><math>\alpha_s</math></b>: bare surface albedo = 0.13 <a href="#">Yang et al. (2013)</a>  <b><math>S_d</math></b>: downward shortwave radiation (<math>W\ m^{-2}</math>) <a href="#">Allan et al. (1998)</a>  <b><math>\epsilon_s</math></b>: bare surface emissivity = 0.95 <a href="#">Tasumi (2003)</a>  <b><math>\epsilon_a</math></b>: atmospheric emissivity <a href="#">Brutsaert (1975)</a>  <b><math>\sigma</math></b>: Stefan-Boltzmann constant (<math>5.67 \times 10^{-8}\ W\ m^{-2}\ K^{-4}</math>)  <b><math>T_a</math></b>: air temperature  <b><math>\rho</math></b>: air density (<math>kg\ m^{-3}</math>)  <b><math>C_p</math></b>: specific heat of air at constant pressure (<math>J\ kg^{-1}\ K^{-1}</math>)  <b><math>r_{a,a}</math></b>: aerodynamic resistance to heat transfer between <math>Z_{om} + d</math> (<math>Z_{om}</math> is the canopy roughness length for momentum transfer, and <math>d</math> is the zero displacement height) and the reference height (<math>m\ s^{-1}</math>). <a href="#">Sánchez, Caselles and Kustas (2008)</a>  <b><math>r_{a,s}</math></b>: aerodynamic resistance to heat flow in the boundary immediately above the soil surface (<math>m\ s^{-1}</math>). <a href="#">Sánchez, Caselles and Kustas (2008)</a>  <b>G</b>: ground heat flux  <b>G/R<sub>n,s</sub></b> is taken to be 0.35 for bare soil surfaces  <b>R<sub>n,s</sub></b>: net radiation for bare soil surfaces (<math>W\ m^{-2}</math>)</p> <p>Based on <a href="#">Yang et al. (2015)</a>:</p> $R_{n,s} = (1 - \alpha_s)S_d + \epsilon_s \epsilon_a \sigma T_a^4 - \epsilon_s \sigma T_s^4$
-------------------------------------------------------------------------------------------------------------------------------------------------------------------------------------------------------------------------------------------------------------------------------------------------------------------------------------------------------------------------------------------------------------------------------------------------------------------------------------------------------------------------------------------------------------------------------------------------------------------------------------------------------------------------------------------------------------------------------------------------------------------------------------------------------------------------------------------------------------------------------------------------------------------------------------------------------------------------------------------------------------------------------------------------------------------------------------------------------------------------------------------------------------------------------------------------------------------------------------------------------------------------------------------------------------------------------------------	--------------------------------------------------------------------------------------------------------------------------------------------------------------------------------------------------------------------------------------------------------------------------------------------------------------------------------------------------------------------------------------------------------------------------------------------------------------------------------------------------------------------------------------------------------------------------------------------------------------------------------------------------------------------------------------------------------------------------------------------------------------------------------------------------------------------------------------------------------------------------------------------------------------------------------------------------------------------------------------------------------------------------------------------------------------------------------------------------------------------------------------------------------------------------------------------------------------------------------------------------------------------------------------------------------------------------------------------------------------------------------------------------------------------------------------------------------------------------------------------------------------------------------------------------------------------------------------------------------------------------------------------------------------------------------------------------------------------------------------------------------------------------------------------------------------------------------------------------------------------------------------------------------------------------------------------------------------------------------------------------------------------------------------------------------------------------------------------------------------------------------------------------------------------------------------------------------------------------------------------------------------------------------------------------------------------

Where:

$\alpha_s$ : bare surface albedo

$S_d$ : downward shortwave radiation ( $\text{W m}^{-2}$ ) [Allan et al.](#) (1998)

$\epsilon_s$ : bare surface emissivity = 0.95 [Tasumi](#) (2003)

$\epsilon_a$ : atmospheric emissivity [Brutsaert](#) (1975)

$\sigma$ : Stefan-Boltzmann constant ( $5.67 \times 10^{-8} \text{ W m}^{-2} \text{ K}^{-4}$ )

$T_a$ : air temperature

$T_s$ : bare surface temperature

$$G = C_G (1 - P_v) R_{ns}$$

Where:

$C_G$  can vary in a range of 0.2–0.5 depending on the soil type and moisture

$P_v$ : fractional vegetation cover without a view angle argument  $\theta$  which refers to the cover fraction at nadir view (i.e.  $\theta = 0^\circ$ )

$R_{ns}$ : contribution of the soil to the total net radiation flux

$$R_{ns} = (1 - \alpha_s) S + \epsilon_s L_{sky} - \epsilon_s \sigma T_s^4$$

Where:

$\alpha_s$ : bare surface albedo

$S$ : solar global radiation ( $\text{W m}^{-2}$ )

$\epsilon_s$ : bare surface emissivity = 0.95 [Tasumi](#) (2003)

$L_{sky}$ : incident long-wave radiation ( $\text{W m}^{-2}$ )

$\sigma$ : Stefan-Boltzmann constant ( $5.67 \times 10^{-8} \text{ W m}^{-2} \text{ K}^{-4}$ )

$T_s$ : bare surface temperature

$$P_v(\theta) = 1 - \exp\left(\frac{-0.5 \Omega(\theta) LAI}{\cos(\theta)}\right)$$

Where:

$P_v$ : fractional vegetation cover without a view angle argument  $\theta$  which refers to the cover fraction at nadir view (i.e.  $\theta = 0^\circ$ )

**$\Omega(\theta)$** : clumping factor to characterize the heterogeneity of the surface. Lower values of  $\Omega$  indicate stronger clumping, while  $\Omega = 1$  for a homogeneous canopy with a random dispersion of leaf area, and  $\Omega > 1$  indicates more regularized distributions. The clumping factor typically varies with the viewing angle, attaining a minimum value at nadir view ( $\Omega_0$ ). [Anderson et al. \(2005\)](#).

**LAI**: Leaf Area Index

$$\Omega(\theta) = \frac{\Omega_0 \Omega_{\max}}{\Omega_0 + (\Omega_{\max} - \Omega_0) \exp(\kappa \theta^p)}$$

Where:

**$\Omega_0$** : minimum value at nadir view

**$\Omega_{\max}$** : approaches unity for an azimuth view perpendicular to the crop row

**$p$**  = 3.8 - 0.46D

**$D$** : ratio between the canopy height and the nominal clump width

**$k$**  = [0.3 + (1.7  $\Omega_0$ )<sup>14</sup>] [Anderson et al. \(2005\)](#).

$$r_{a,a} = \frac{\left[ \text{Ln} \left( \frac{z_u - d}{z_{0M}} \right) - \Psi_M \right] \left[ \left[ \text{Ln} \left( \frac{z_u - d}{z_{0M}} \right) - \Psi_H \right] \right]}{k^2 u}$$

Where:

**$r_{a,a}$** : aerodynamic resistance to heat transfer between  $Z_{om} + d$  ( $Z_{om}$  is the canopy roughness length for momentum transfer, and  $d$  is the zero displacement height) and the reference height ( $\text{m s}^{-1}$ ). [Sánchez, Caselles and Kustas \(2008\)](#)

**$Z_u$** : measurement heights (m) for wind speed

**$Z_{0M}$** : canopy roughness length for momentum (m)  $z_{0M} = h / 10$

**$d$** : Displacement height  $d = 2h / 3$  ( $h$ : canopy height)

**$\Psi_M$** : stability functions for momentum [Brutsaert \(1999\)](#)

**$\Psi_H$** : stability functions for heat [Brutsaert \(1999\)](#)

**$K$** : Von Karman constant ( $\approx 0.41$ )

**$u$** : wind speed ( $\text{m s}^{-1}$ )

	$r_a^s = \frac{1}{0.0025(T_s - T_c)^{1/3} + 0.012u_s}$ <p>Where:  <b>r<sub>s,a</sub></b>: aerodynamic resistance to heat flow in the boundary layer immediately above the soil surface  <b>u<sub>s</sub></b>: wind speed at height above the soil surface where the effect of soil surface roughness on the free wind movement can be neglected</p>	
<b>Radiation Stress</b>	Not accounted for	<b>Accounted for in WaPOR ETLook Model</b> Computes the stress for plants when there is not sufficient radiation $RS = \frac{ra_{24}}{(ra_{24} + 60)} \times \left(1 + \frac{60}{500}\right)$ <p>Where:  <b>RS</b>: Radiation Stress factor  <b>ra<sub>24</sub></b> : daily solar radiation (W/m<sup>2</sup>)          Solar radiation is derived using MSG and the DEM. The MSG shortwave radiation product is used to calculate daily transmissivity. The reason for not using the MSG shortwave radiation data directly is because of the limited resolution (&gt; 3km) and of the lack of surface relief effects. The slope and aspect maps derived from the DEM are used to calculate the solar radiation for inclined surfaces, based on Tasumi, et al. (2006</p>
<b>Temperature Stress (TS)</b>	<b>Accounted for in GYMEE Biomass Model:</b> $TS = \frac{(T - T_L) \times (T_H - T)^{Jc}}{(K_T - T_L) \times (T_H - K_T)^{Jc}}$ <p>Where:  <b>TS</b>: Plant Temperature Constraint  <b>T</b>: daily temperature</p>	<b>Accounted for in WaPOR ETLook Model</b> $S_T = \frac{(T_a - T_{min}) \times (T_{max} - T_a)^f}{(T_{opt} - T_{min}) \times (T_{max} - T_{opt})^f}$ <p>Where:  <b>T<sub>a</sub></b>: daily air temperature  <b>T<sub>opt</sub></b>: 25: optimum air temperature for plant growth</p>

	<p><b>T<sub>H</sub></b>: upper limit of stomatal activity = 45  <b>T<sub>L</sub></b>: lower limit of stomatal activity = 0  <b>K<sub>T</sub></b>: Optimum conductance temperature (°C) = 24  <i>J<sub>C</sub></i>: Jarvis Coefficient</p>	<p><b>T<sub>min</sub></b>: 0: minimum air temperature for plant growth  <b>T<sub>max</sub></b>: 50: maximum air temperature for plant growth  <math display="block">f = \frac{T_{max} - T_{opt}}{T_{opt} - T_{min}}</math> (WaPOR Data Manual Evapotranspiration V2, Final Draft 2.2, 2020)</p>
Jarvis Coefficient	$J_C = \frac{T_H - K_T}{K_T - T_L}$ <p><b>T<sub>H</sub></b> = 45  <b>T<sub>L</sub></b> = 0  <b>K<sub>T</sub></b> = 24</p>	$J_C = \frac{T_H - K_T}{K_T - T_L}$
Vapor Stress (VS)	<p><b>Accounted for in GYMEE Biomass Model:</b></p> $VS = 0.88 - 0.183 \times \log(e_s \times e_a)$ <p>Where:  <b>e<sub>s</sub></b>: saturated vapor pressure  <b>e<sub>a</sub></b>: actual vapor pressure</p>	<p><b>Accounted for in WaPOR ETLook Model</b>  Computes the stress for plants if the VPD increases too much.  With lower slopes the stress increases faster  <math display="block">VS = vpd_{slope} \times \ln(0.1 \times vpd_{24} + 0.5) + 1</math> Where:  <b>VS</b>: Vapor Stress - stress factor for vapor pressure deficit  <b>vpd<sub>slope</sub></b>: -0.3: vapor pressure stress curve slope  <b>vpd<sub>24</sub></b>: daily vapor pressure deficit (mbar)</p>
		<p><b>vpd<sub>24</sub></b> is computed by deriving the vapor pressure deficit  Δe in [mbar]: Δe = e<sub>s</sub> - e<sub>a</sub> but as a daily average  <b>e<sub>s</sub></b>: saturated vapor pressure  <b>e<sub>a</sub></b>: actual vapor pressure</p>

	$vpd_{slope} = \left( \frac{4098 \times e_s}{237.3 + T} \right)^2$ <p>Where:  <b><math>e_s</math></b> : Saturated vapor pressure  <b><math>T</math></b> : air temperature</p>
	$e_s = 6.108 \times e^{\left( \frac{17.27 \times T}{237.3 + T} \right)}$ <p>Where:  <b><math>e_s</math></b> : Saturated vapor pressure  <b><math>T</math></b> : air temperature</p>

## APPENDIX 2

Economic inputs include costs of fertilizers, pesticides, seeds or cuttings, diesel, operation, labor, and land rental.

Fertilizers cost: Refers to the expenses incurred in purchasing fertilizers (USD) per 1 hectare of cultivated crop per growing season as per the local farmers' cultural practices in the basin.

Pesticides cost: Refers to the expenses incurred in purchasing pesticides (USD) per 1 hectare of cultivated crop per growing season as per the local farmers' cultural practices in the basin.

Diesel cost: Indicates the cost of diesel fuel used in fueling and operating irrigation pumps and systems, per crop per growing season (USD/ha).

Operation cost: Includes expenses directly associated with crop production such as costs of plowing, spraying, pruning, and tractor works (USD/ha) of cultivated crop per growing season.

Seeds/ cuttings cost: Refers to the expenses involved in purchasing seeds for planting crops per season (USD/ha). For table grapes, the initial cost of cuttings is annualized over 20 years.

Land rental cost: Represents the cost incurred by farmers or producers for renting or leasing agricultural land for crop cultivation per district in USD/ha.

Labor cost: Refers to the expenses associated with labor wages for agricultural workers involved in various tasks, including planting, harvesting, irrigation, pest control, and other farm operations in USD/ha. The labor cost adheres to the prevailing local pay range commonly observed in the three districts of the basin.

## REFERENCES

- Adeboye, O. B., Schultz, B., Adekalu, K. O., & Prasad, K. (2015). Crop water productivity and economic evaluation of drip-irrigated soybeans (*Glyxine max* L. Merr.). *Agriculture & Food Security*, 4(1), 1-13.
- Alexandratos, N., & Bruinsma, J. (2012). World agriculture towards 2030/2050: the 2012 revision.
- Arnold, J. G., Srinivasan, R., Muttiah, R. S., & Allen, P. M. (1999). Continental scale simulation of the hydrologic balance 1. *JAWRA Journal of the American Water Resources Association*, 35(5), 1037-1051.
- ASCE. (1996). *Hydrology Handbook*. Retrieved from
- Bashe, T., Alamirew, T., & Dejen, Z. A. (2022). Estimating the economic value and economic return of irrigation water as a sustainable water resource management mechanism. *Sustainable Water Resources Management*, 8(6), 175.
- Bastiaanssen, W., Cheema, M., Immerzeel, W., Miltenburg, I., & Pelgrum, H. (2012). Surface energy balance and actual evapotranspiration of the transboundary Indus Basin estimated from satellite measurements and the ETLook model. *Water Resources Research*, 48(11).
- Bellù, L. G. (2013). Value chain analysis for policy making. *Methodological Guidelines and country cases for a Quantitative Approach*. Roma: Food and Agriculture Organization.
- Biradar, C. M., Thenkabail, P. S., Platonov, A., Xiao, X., Geerken, R., Noojipady, P., . . . Vithanage, J. (2008). Water productivity mapping methods using remote sensing. *Journal of Applied Remote Sensing*, 2(1), 023544.
- Blatchford, M. L., Mannaerts, C. M., Zeng, Y., Nouri, H., & Karimi, P. (2019). Status of accuracy in remotely sensed and in-situ agricultural water productivity estimates: A review. *Remote sensing of environment*, 234, 111413.
- Bos, M. G., Burton, M. A., & Molden, D. J. (2005). *IRRIGATION AND DRAINAGE PERFORMANCE ASSESSMENT Practical Guidelines*: CABI.
- Carlson, T. (2007). An overview of the “triangle method” for estimating surface evapotranspiration and soil moisture from satellite imagery. *Sensors*, 7(8), 1612-1629.
- Droogers, P., Malik, R., Kroes, J., Bastiaanssen, W. G., & Van Dam, J. (2003). Future water management in Sirsa district: options to improve water productivity *Water productivity of irrigated crops in Sirsa district, India; integration of remote sensing, crop and soil models and geographical information systems* (pp. 135-156): Wageningen UR etc.
- FAO. (2020). *WaPOR database methodology: Version 2 release, April 2020*. Retrieved from Rome:
- FAO. (2023). *FAO pyWaPOR ETLook and Biomass Data Manual and Algorithm*. Retrieved from: [https://bitbucket.org/cioapps/pywapor/src/master/pywapor/et\\_look\\_v2\\_v3/](https://bitbucket.org/cioapps/pywapor/src/master/pywapor/et_look_v2_v3/)
- FAO, & World Bank. (2022). *Irrigating from space – Using remote sensing for agricultural water management*. Retrieved from Rome:
- Fensholt, R., Sandholt, I., & Rasmussen, M. S. (2004). Evaluation of MODIS LAI, fAPAR and the relation between fAPAR and NDVI in a semi-arid environment using in situ measurements. *Remote sensing of environment*, 91(3-4), 490-507.

- Fernández, J., Alcon, F., Diaz-Espejo, A., Hernandez-Santana, V., & Cuevas, M. (2020). Water use indicators and economic analysis for on-farm irrigation decision: A case study of a super high density olive tree orchard. *Agricultural Water Management*, 237, 106074.
- Fitton, N., Alexander, P., Arnell, N., Bajzelj, B., Calvin, K., Doelman, J., . . . Herrero, M. (2019). The vulnerabilities of agricultural land and food production to future water scarcity. *Global Environmental Change*, 58, 101944.
- Foley, D. J., Thenkabail, P. S., Aneece, I. P., Teluguntla, P. G., & Oliphant, A. J. (2020). A meta-analysis of global crop water productivity of three leading world crops (wheat, corn, and rice) in the irrigated areas over three decades. *International Journal of Digital Earth*, 13(8), 939-975.
- FRAME. (2020). *FAO WaPOR V2 Documentation*. Retrieved from: [https://bitbucket.org/cioapps/wapor-et-look/src/master/version2\\_documentation/](https://bitbucket.org/cioapps/wapor-et-look/src/master/version2_documentation/)
- Goward, S. N., & Huemmrich, K. F. (1992). Vegetation canopy PAR absorptance and the normalized difference vegetation index: an assessment using the SAIL model. *Remote sensing of environment*, 39(2), 119-140.
- Guzinski, R., & Nieto, H. (2019). Evaluating the feasibility of using Sentinel-2 and Sentinel-3 satellites for high-resolution evapotranspiration estimations. *Remote sensing of environment*, 221, 157-172.
- Hanan, N., Prince, S., & Bégué, A. (1995). Estimation of absorbed photosynthetically active radiation and vegetation net production efficiency using satellite data. *Agricultural and forest meteorology*, 76(3-4), 259-276.
- Hellegers, P. J., Soppe, R., Perry, C. J., & Bastiaanssen, W. G. (2010). Remote sensing and economic indicators for supporting water resources management decisions. *Water resources management*, 24, 2419-2436.
- Jaafar, H., & Ahmad, F. (2020). Time series trends of Landsat-based ET using automated calibration in METRIC and SEBAL: The Bekaa Valley, Lebanon. *Remote sensing of environment*, 238, 111034.
- Jaafar, H., Ahmad, F., Holtmeier, L., & King-Okumu, C. (2020). Refugees, water balance, and water stress: Lessons learned from Lebanon. *Ambio*, 49(6), 1179-1193. doi:10.1007/s13280-019-01272-0
- Jaafar, H., King-Okumu, C., Haj-Hassan, M., Abdallah, C., El-Korek, N., & Ahmad, F. (2016). *Water resources within the Upper Orontes and Litani Basins - A balance, demand and supply analysis amid the Syrian refugees crisis*. Retrieved from London: <https://www.iiied.org/sites/default/files/pdfs/migrate/10174IIED.pdf>
- Jaafar, H., & Mourad, R. (2021). GYMEE: a global field-scale crop yield and ET mapper in Google Earth Engine based on Landsat, weather, and soil data. *Remote Sensing*, 13(4), 773.
- Jaafar, H., Mourad, R., & Schull, M. (2022). A global 30-m ET model (HSEB) using harmonized Landsat and Sentinel-2, MODIS and VIIRS: Comparison to ECOSTRESS ET and LST. *Remote sensing of environment*, 274, 112995.
- Jarvis, P. (1976). The interpretation of the variations in leaf water potential and stomatal conductance found in canopies in the field. *Philosophical Transactions of the Royal Society of London. B, Biological Sciences*, 273(927), 593-610.
- Kang, S., Hao, X., Du, T., Tong, L., Su, X., Lu, H., . . . Ding, R. (2017). Improving agricultural water productivity to ensure food security in China under changing environment: From research to practice. *Agricultural Water Management*, 179, 5-17.

- Kuzma, S., Saccoccia, L., & Chertock, M. (2023). 25 Countries, Housing One-quarter of the Population, Face Extremely High Water Stress.
- McShane, R. R., Driscoll, K. P., & Sando, R. (2017). A review of surface energy balance models for estimating actual evapotranspiration with remote sensing at high spatiotemporal resolution over large extents. *Scientific Investigations Report*(2017-5087).
- Molden, D., Oweis, T. Y., Pasquale, S., Kijne, J. W., Hanjra, M. A., Bindraban, P. S., . . . Upadhyaya, A. (2007). Pathways for increasing agricultural water productivity.
- Monteith, J. L. (1972). Solar radiation and productivity in tropical ecosystems. *Journal of applied ecology*, 9(3), 747-766.
- Myneni, R. B., Hoffman, S., Knyazikhin, Y., Privette, J., Glassy, J., Tian, Y., . . . Smith, G. (2002). Global products of vegetation leaf area and fraction absorbed PAR from year one of MODIS data. *Remote sensing of environment*, 83(1-2), 214-231.
- Myneni, R. B., & Williams, D. (1994). On the relationship between FAPAR and NDVI. *Remote sensing of environment*, 49(3), 200-211.
- Nouri, H., Stokvis, B., Borujeni, S. C., Galindo, A., Brugnach, M., Blatchford, M., . . . Hoekstra, A. (2020). Reduce blue water scarcity and increase nutritional and economic water productivity through changing the cropping pattern in a catchment. *Journal of Hydrology*, 588, 125086.
- Perry, C. (2007). Efficient irrigation; inefficient communication; flawed recommendations. *Irrigation and Drainage: The Journal of the International Commission on Irrigation and Drainage*, 56(4), 367-378.
- Prince, S. D., & Goward, S. N. (1995). Global primary production: a remote sensing approach. *Journal of biogeography*, 815-835.
- Ruimy, A., Saugier, B., & Dedieu, G. (1994). Methodology for the estimation of terrestrial net primary production from remotely sensed data. *Journal of Geophysical Research: Atmospheres*, 99(D3), 5263-5283.
- Running, S. W., Nemani, R., Glassy, J. M., & Thornton, P. E. (1999). MODIS daily photosynthesis (PSN) and annual net primary production (NPP) product (MOD17) Algorithm Theoretical Basis Document.
- Safi, A. R., Karimi, P., Mul, M., Chukalla, A., & De Fraiture, C. (2022). Translating open-source remote sensing data to crop water productivity improvement actions. *Agricultural Water Management*, 261, 107373.
- Sánchez, J., Kustas, W., Caselles, V., & Anderson, M. (2008). Modelling surface energy fluxes over maize using a two-source patch model and radiometric soil and canopy temperature observations. *Remote sensing of environment*, 112(3), 1130-1143.
- Santos, C., Lorite, I. J., Tasumi, M., Allen, R. G., & Fereres, E. (2010). Performance assessment of an irrigation scheme using indicators determined with remote sensing techniques. *Irrigation Science*, 28, 461-477.
- Schmitz, C., Lotze-Campen, H., Gerten, D., Dietrich, J. P., Bodirsky, B., Biewald, A., & Popp, A. (2013). Blue water scarcity and the economic impacts of future agricultural trade and demand. *Water Resources Research*, 49(6), 3601-3617.
- Steduto, P., Raes, D., Hsiao, T. C., Fereres, E., Heng, L. K., Howell, T. A., . . . Izzi, G. (2009). *Concepts and applications of AquaCrop: The FAO crop water productivity model*. Paper presented at the Crop modeling and decision support.
- Stewart, J. (1987). On the use of the Penman-Monteith equation for determining area! évapotranspiration. *Estimation Areal Evapotranspiration*, 3-12.

- Stewart, J. (1988). Modelling surface conductance of pine forest. *Agricultural and forest meteorology*, 43(1), 19-35.
- Stockle, C. O., Martin, S. A., & Campbell, G. S. (1994). CropSyst, a cropping systems simulation model: water/nitrogen budgets and crop yield. *Agricultural systems*, 46(3), 335-359.
- Swinnen, E., Van Hoolst, R., & Toté, C. (2019). Copernicus global land operations “vegetation and energy” quality assessment report for dry matter productivity (DMP) and gross dry matter productivity (GDMP). Collection 1 km, version 2. Brussels, Belgium: Collection.
- Tawk, S. T., Chedid, M., Chalak, A., Karam, S., & Hamadeh, S. K. (2019). Challenges and sustainability of wheat production in a Levantine breadbasket: The case of the West Bekaa, Lebanon. *Journal of Agriculture, Food Systems, and Community Development*, 8(4), 193-209.
- Tubiello, F., Schmidhuber, J., Howden, M., Neofotis, P. G., Park, S., Fernandes, E., & Thapa, D. (2008). Climate change response strategies for agriculture: challenges and opportunities for the 21st century. *Agriculture and rural development discussion paper*, 42.
- Uhlenbrook, S., Yu, W., Schmitter, P., & Smith, D. M. (2022). Optimising the water we eat—rethinking policy to enhance productive and sustainable use of water in agri-food systems across scales. *The Lancet Planetary Health*, 6(1), e59-e65.
- Veroustraete, F., Sabbe, H., & Eerens, H. (2002). Estimation of carbon mass fluxes over Europe using the C-Fix model and Euroflux data. *Remote sensing of environment*, 83(3), 376-399.
- Xue, J., Anderson, M. C., Gao, F., Hain, C., Sun, L., Yang, Y., . . . Schull, M. (2020). Sharpening ECOSTRESS and VIIRS land surface temperature using harmonized Landsat-Sentinel surface reflectances. *Remote sensing of environment*, 251, 112055.
- Yang, Y., Guan, H., Long, D., Liu, B., Qin, G., Qin, J., & Batelaan, O. (2015). Estimation of surface soil moisture from thermal infrared remote sensing using an improved trapezoid method. *Remote Sensing*, 7(7), 8250-8270.
- Young, R. A., & Loomis, J. B. (2014). *Determining the economic value of water: concepts and methods*: Routledge.
- Zisopoulou, K., Zisopoulos, D., & Panagoulia, D. (2022). Water economics: An in-depth analysis of the connection of blue water with some primary level aspects of economic theory I. *Water*, 14(1), 103.
- Zwart, S. J., & Bastiaanssen, W. G. (2004). Review of measured crop water productivity values for irrigated wheat, rice, cotton and maize. *Agricultural Water Management*, 69(2), 115-133.